energies

MDPI

*Article*

# Experimental Study of Fracture Propagation: The Application in Energy Mining

**Yuxiang Cheng and Yanjun Zhang ***

Construction Engineering College, Jilin University, Ximinzhu Street, Changchun 130000, China; chengyx16@mails.jlu.edu.cn
* Correspondence: zhangyanj@jlu.edu.cn; Tel.: + 86-1894-314-2020

Received: 14 January 2020; Accepted: 14 March 2020; Published: 18 March 2020

**Abstract:** Hydraulic fracturing has been widely used in recent years as a key technology to improve energy mining efficiency in petroleum and geothermal industries. Laboratory hydraulic fracturing experiments recently were completed in six large-scale 300 × 300 × 300 mm rock specimens to better understand this complex process of hydraulic fracturing. When injection flow rate increases from 5 to 30 mL/min. The fracture initiation pressures and breakdown pressures increase, the propagation times and post-fracturing pressures decrease. The fracture geometries are observed and analyzed, mean injection power is proposed and results show that it could be used to roughly estimate the fracture total lengths. Moreover, the fracture permeabilities based on the pressure data are calculated and linearly ascend with the increase of injection flow rates. These results can provide some reasonable advice for implementing hydraulic fracturing reservoir simulations and improving energy production efficiency on application to field-scale operation.

**Keywords:** hydraulic fracturing; injection flow rate; rock; pressure

## 1. Introduction

Hydraulic fracturing has been widely used in recent years as a key technology to improve energy mining efficiency in petroleum and geothermal industries [1–4]. The environmental impact of hydraulic fracturing has also gained considerable attention with scientific community and policy makers [5–8]. The hydraulic fracturing process involves drilling a hole deep into a layer of rock [9]. The fluid is pumped under high pressure into rocks to fracture and enhance the reservoir connectivity [10]. When conducting hydraulic fracturing stimulation in a field scale reservoir, the fracturing injection flow rate is an important element to consider [9,11,12]. The injection flow rate and injection pressure are also the critical operating parameter for the effective design of hydraulic fracturing process [13–15]. At the same time, reservoirs are deeply buried, making it difficult to carry out in situ hydraulic fracturing experiments. Thus, it is necessary to use laboratory experiment consequences for aided analysis and evaluations. The laboratorial hydraulic fracturing experiment usually involves drilling a borehole in a rock sample, an injection tube is sealed in the hole, and then fluid is injected to induce fractures.

In order to optimize reservoir stimulation, several researchers have conducted studies about the mechanism of hydraulic fracturing. They have shown that, in the fracture initiation and propagation process, the flow rate and fluid pressure play important roles [15–27]. Hubbert and Willis [16] first studied the hydraulic fracturing mechanism, and proposed a stress formula for hydraulic induced fracture initiation, and they found that fracture and breakdown pressures are affected by the pre-existing regional stresses. A similar hydraulic fracture initiation criterion was also proposed by Haimson and Fairhurst [17], they found that the fracture volume was a function of the injection rate. These researchers also [16–18] found that the fractures propagation direction should be approximately perpendicular to the direction of least principle stress. Zoback et al. [15] first conducted hydraulic fracturing on cubic intact and pre-fractured rock, and showed that the breakdown process was influenced by the rate of borehole pressurization. Solberg et al. [19,20] first conducted low-permeability granite hydraulic fracturing experiment under high temperature with small cylindrical samples, they showed that the injection flow rate could influence fracture's patterns, both shear and tension fractures could be initiated when hydraulic injection pressure was changed. Luke et al. [21] first performed an experimental study on an intact granite rock reservoir and demonstrate reservoir environment can be created in laboratory, an intact rock could be hydraulic fractured in an appropriate injection flow rate, acoustic emission sensors can be used to analyze hydraulic induced fracture propagation, and the reservoir permeability is obviously increased. Guo et al. [11] showed that breakdown pressure could be used to calculate the horizontal stresses, and the breakdown pressure was influenced by injection flow rate, in situ stresses, reservoir size, fracturing fluid, etc. Similar results also were found by other researchers [22–25], the injection flow rate could influence the hydraulic fracturing pump pressure and fracture patterns. Fallahzadeh et al. [25] performed hydraulic fracturing tests in 150 mm synthetic cubic samples and show that with the increasing of flow rate, the initiation angle of fracture increased and resulted in a more curved plane. Nagel et al. [26] found that a higher injection flow rate trended to create tensile failure, whereas a lower injection flow rate would create shear fracture. Zhang and Jeffrey [27] simulated the hydraulic fracturing process through different injection rates and found that constant injection rate is more possible to create a fracture network than constant injection pressure. These studies show that the injection flow rate affects the inject pump pressure and fracture propagation of hydraulic fracturing, it is necessary to conduct large-scale granite laboratorial experiments to study the hydraulic fracturing characteristics.

Additionally, several numerical simulation studies have also been conducted to numerical simulation and analyze the fracture creation and propagation mechanism. Al-Busaidi et al. [28] established hydraulic fracturing numerical models on the basis of a multi-dimensional Particle Flow Code Model, they simulated the variety of propagation and interactions different kind of fractures. Weng et al. [29] numerically simulated a pre-existing discrete fracture network with variable injection-rate methods, their numerical modeling results showed that the combination of different injection-rate methods is a good technology to form a complex fracturing network. Rothert and Shapiro [30] proposed a numerical modeling method based on a diffusive process of pore-pressure relaxation in subcritically stressed rocks and presented the spatio-temporal distributions of micro-fracture events. Rahman et al. [31] simulated the coupling process of fluid and rock during hydraulic fracturing through the finite element method. Guo et al. [32] simulated radial hydraulic propagation and its factors on the propagation of hydraulic fracturing, established a single radial borehole model. Pakzad et al. [33] proposed a numerical model and predict the behavior of a block with different permeabilities under different confining stress conditions and pressurization rates.

Although a large number of works have been carried out to analyze the hydraulic fracturing influencing factors, the results were still inconsistent. Previous studies on large scale hydraulic fracturing were mostly conducted on artificial cement samples with artificial materials such as cement mortar, concrete and Perspex [34,35]. Even though some studies used real natural rocks, most of the experiments used small cylindrical rock samples with 50–60 mm in diameter and 100–120 mm in height for hydraulic fracturing under a pseudo triaxial confining stress state [36–38]. The tensile and shear strengths of cement samples were much lower than that of granites. Smaller pressure could trigger the fracture and form a fracture network. Therefore, even large-sized cement samples were easily fractured under laboratory conditions. The fracturing results obtained by replacing granite with cement were probably not consistent with the actual fracturing condition of granite. For small cylindrical or cubic granite samples, because of the small sample size, the required fracturing pressure was small, and the formation of the fracture network was also limited. Because of the small size of the specimen, it is usually difficult to determine the morphology of the fracture changes and the fracturing results are not in good agreement with the field site fracturing consequences. As a result, these conclusions were often difficult to apply in field-scale hydraulic fracturing to guide the field scale project.

Hydraulic fracturing usually relates complicated solid–fluid coupling processes. Due to the compactness and the low permeability of the granite, an intact large-size granite sample requires a high fracturing pressure to trigger the fracture. To better understand the characteristics of hydraulic fracturing process and fracture network after hydraulic fracturing. In this work, we carried out laboratorial hydraulic fracturing experiments with a true triaxial fracturing apparatus designed by Jilin University. Its cubic specimen fracturing capsule size is 300 × 300 × 300 mm. The granite samples were collected from the Songliao Basin petroleum reservoir field in the northeastern part of China. In order to investigate the injection flow rate on hydraulic fracturing chrematistics, we conducted hydraulic fracturing tests at different injection flow rates for six rocks. The initiation pressure, breakdown pressure, post-fracturing pressure, and propagation time were analyzed based on the fracturing pressure curves. The rock specimens were cut in half after test and the fracture geometry was observed. Based on recorded pressure data and curves, the fracture permeabilities of all specimens were calculated. Results in this study could provide some reasonable advice for implementing hydraulic fracturing reservoir simulations and improving energy production efficiency on application to field-scale operation.

## 2. Laboratorial Tests

### *2.1. Background*

The granite samples used in this study are taken from a place nearby YS-2 well (Figure 1) in the Songliao Basin [39]. The YS-2 well (127.25 °E, 52.36 °N) is in the Daqing Oilfield about 78 km from Daqing City, The YS-2 well is a geothermal energy exploration well, and exploration data shows that the geothermal resources here are abundant. As large size intact rock samples cannot be gotten from a wellbore. We use the outcrop rock samples as substitutes (Figure 2a). Three independent triaxial principal stresses are applied on cube-shaped samples to simulate the real field in-situ stress conditions, the rocks are cut into 300 × 300 × 300 mm cubes. The outcrops were cut into 300 × 300 × 300 mm cubes (Figure 2b). The mineral composition and basic physical properties of the rock specimens were measured (Tables 1 and 2). A total of ten small granite samples were used for mineral composition and rock properties testing. All of these ten samples were rock debris from cutting outcrops into cube-shaped samples. It meant that the properties and mineral compositions of these ten samples were the same with the aforementioned six large cubic samples. All of the physical property and mineral composition tests were conducted in the Environment and Groundwater Resources Education Ministry Key Laboratory of Jilin University. The rock property testing results were shown in Table 1, the property range indicated the minimum and maximum in each property test, average value represented the average property value in each test. Each mineral had a specific X-ray diffraction spectrum, the characteristic peak intensity in the spectrum was related to the content of minerals, then the mineral qualitative and quantitative composition could be obtained, the rock debris was processed into rock powder, and the X-ray diffraction test analysis was conducted to obtain the mineral compositions which were shown in Table 2.

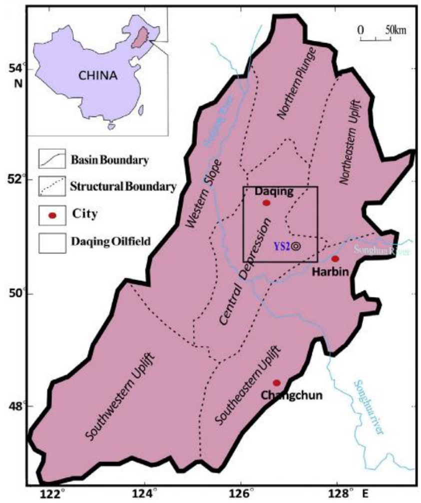


**Figure 1.** The Songliao Basin map with the location of the Daqing Oilfield and YS-2 well.

(**a**) (**b**)

**Figure 2.** (**a**) A complete outcrop rock sample and (**b**) the outcrop rock sample were cut into 300 × 300 × 300 mm cubes.

**Table 1.** Physical properties of rock samples.

| Property | Range | Average Value |
|---|---|---|
| Density [1], ρ (g/cm$^3$) | 2.4–2.7 | 2.5 |
| Porosity [1], ϕ (%) | 2.49–4.59 | 3.22 |
| Permeability [1], K (mD) | 0.27–0.52 | 0.34 |
| Thermal conductivity [1] (W·m$^{-1}$·K$^{-1}$) | 1.75–3.00 | 2.48 |
| Specific heat [1] (J·kg$^{-1}$·K$^{-1}$) | 709–800 | 736 |
| Poisson's ratio [1], ν | 0.14–0.35 | 0.28 |
| Elastic modulus [1], E (GPa) | 28.11–56.04 | 39.99 |
| shear modulus [1],G (GPa) | 10.54–21.84 | 15.86 |
| Shear wave velocity [1], $V_s$ (mm/µs) | 2.02–2.89 | 2.47 |
| Compression wave velocity [1], $V_p$ (mm/µs) | 3.57–5.25 | 4.45 |
| Unconfined compression strength, UCS (MPa) | N/A | 152 |
| Brazilian tensile strength [1], BTS (MPa) | 11.05–24.08 | 17.14 |
| Shear strength [1], SS(MPa) | 20.00–27.00 | 22.60 |
| Cohesive force [1], $C_0$ (MPa) | 10.19–13.75 | 11.71 |
| The angle of internal friction [1], φ (°) | 48.3–49.4 | 48.9 |

[1] Data includes tests performed by the authors.

**Table 2.** Mineral composition of rock samples.

| Mineral Composition | Value |
|---|---|
| Quartz | 0.35 |
| Potash Feldspar | 0.23 |
| Plagioclase | 0.30 |
| Others | 0.12 |

### 2.2. Rock Sample Preparation

The following procedures used for the preparation of rock sample were shown in Figure 3: (1) The rocks were cut into 300 × 300 × 300 mm cubes with a perpendicularity of ±1°, surface tolerance of ±1 mm, the ones with higher homogeneity and more intact ones are preferred; (2) A borehole was drilled in the center of the rock's surface, with the depth of 150 mm, and the wellbore bottom was in the center of the rock sample; (3) the wellbore was drilled at 700 rpm using a 15 mm masonry drill bit, to prevent drilling caused micro cracks around the wellbore, drilling was began as soon as the sample was removed from the water bath; (4) After the drilling, distilled water was used to flush the borehole until cleaning up all the rock debris in the borehole; (5) After the distilled water in the wellbore completely evaporated and the wellbore wall was dry, the epoxy grout resin adhesive was injected into the wellbore; (6) The water injection tube (Figure 3c) was a hollow stainless steel tube with a 10 mm outside diameter, a 160mm length, the tube was slightly roughened to provide a better bond between the tube, adhesive and rock and the maximum internal pressure that the tube could withstand is 60 MPa; (7) The injection tube was design to have two side holes for fluid to flow through to fracture the rock near the bottom; (8) A transparent plastic was sealed on the side holes to prevent the adhesive flowing into the injection tube, then the tube was pressed into the wellbore to be glued, 150 mm of the tube was stuck into the rock sample, the transparent plastic prevented adhesive flowing into the tube; (9) 10 mm of the tube, as a water injection hole, was exposed outside the rock sample, then water flowed into the rock through the exposed part, when the water was pressured into the tube, the plastic fails, and water flowed into the rock; (10) After the injection tube and rock were glued, they were placed at room temperature for more than 48 hours, so that the tube and the rock were completely bonded.

Due to the compactness and the low permeability of the granite, an intact large-size granite sample requires a high fracturing pressure to trigger the fracture. The main difficulty in the experiment is how to seal the well tube and the rock. We need ensure the adhesive has sufficient resistance to high injection pressure. The adhesive strength should be much higher than the maximum fracturing pressure, and the glue needs to completely wrap the injection tube, there is no adhesive weak point around the injection tube, the colloidal properties are stable at high temperature, and all the injected water will be forced into the rock during the fracturing process.

In order to make the epoxy grout resin adhesive better glue the tube and withstand higher water pressure. After many experiments, we find a gluing process, which can guarantee sufficient adhesive strength between the wellbore and tube. Some matters for attention are put forward: (1) After the well is drilled, the rock debris may be left in the well, to prevent the adhesive weak point because of the rock debris, the inside wall of the wellbore must be washed by distilled water, the tube can be glued after the water in the wellbore is completely dry; (2) The wellbore diameter is slightly larger than the injection tube outside diameter, a narrow annulus (about 2 mm) between the wellbore and tube is considered for the placement of adhesive, there will be enough space for the adhesive filling the annulus, the tube can be completely wrapped by the adhesive, the narrow annulus also could not only minimize the effect of adhesive on stress distribution in tube and wellbore, but also provide enough bond stress to prevent water leakage from the annulus during hydraulic fracturing under triaxial stresses; and (3) The usual method to glue the tube is to apply the adhesive around the tube, then the tube is inserted into the wellbore, during the whole process, the adhesive around the tube is easy to touch the inside wall of the wellbore, forming weak bond points. As a result, the adhesive cannot withstand high pressure, the water may flow out along annulus, and no fractured is induced. Hence we propose an improved adhesive method. The adhesive has high viscosity and is not easy to fill and seal the annulus between the tube and wellbore. To resolve this problem, initially the adhesive is put into a syringe with a long needle. The needle should be longer than the depth of the wellbore. The adhesive is carefully injected from the wellbore bottom, as the adhesive rises, the syringe is gradually lifted until there is enough adhesive in the wellbore. Then the tube is slowly inserted into the wellbore, firmly pushed against the bottom of the wellbore for bonding, the adhesive flowed upward and out of the wellbore from the annulus, filling the whole space between tube and wellbore and the excess adhesive is wiped off. The upward flow adhesive ensures that there is no air bubble left in the narrow annulus and the sealing of the dried adhesive is consequently guaranteed.

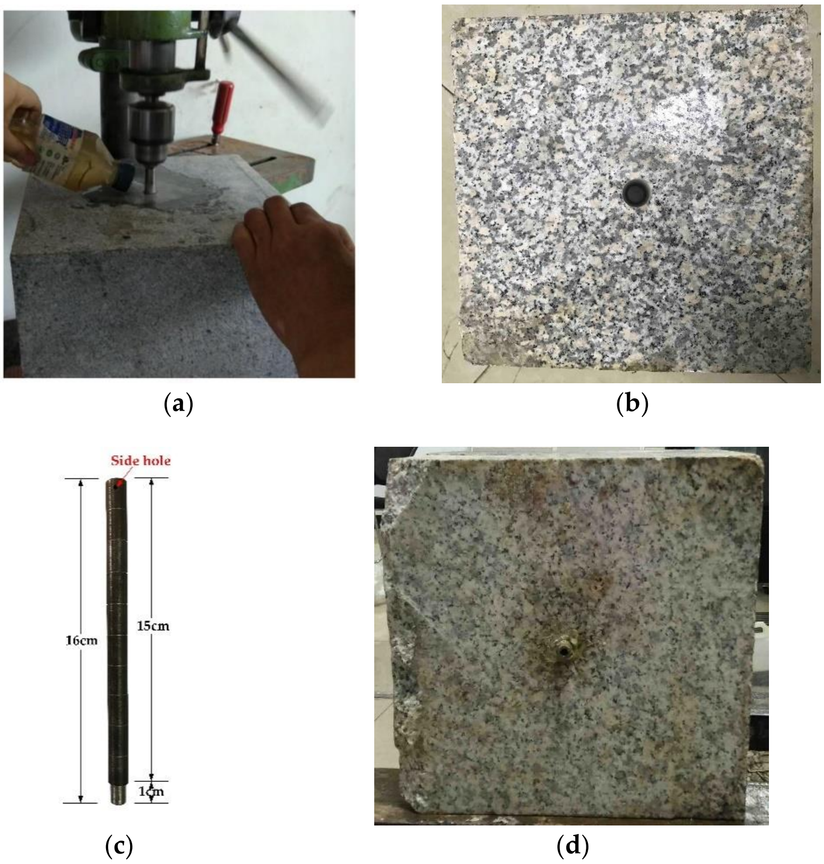


**Figure 3.** Rock sample preparation: (**a**) Drilling the borehole; (**b**) a rock sample after drilling the borehole; (**c**) the water injection tube; and (**d**) a prepared rock sample.

## 2.3. Hydraulic Fractruing Experimential Equipment

The tests were conducted on a true-triaxial hydraulic fracturing apparatus that was developed by Jiangsu Nantong Petroleum Instrument Co. Ltd and the Environment and Groundwater Resources Education Ministry Key Laboratory in Jilin University. The fracturing apparatus has two advantages, one that it has a heating device to provide temperature high enough to simulate the enhanced geothermal system (EGS) temperature environment, the other one is that it could provide triaxial principal to simulate in situ stresses. The apparatus main components are shown in Figure 4. It consists of four sub-systems: a water injection system, a heating system, a steel framework and confining pressure system, and a computer monitor system.

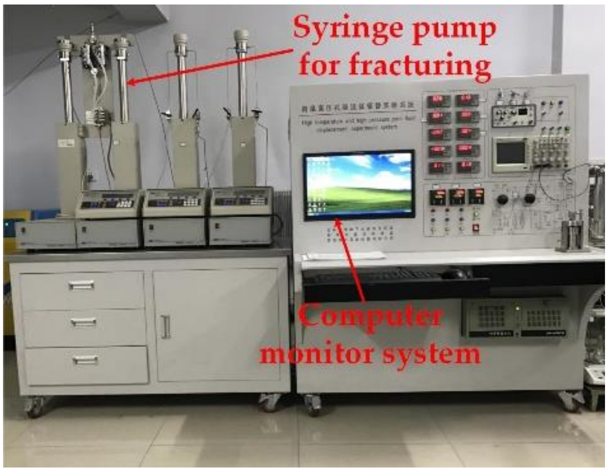


(a)

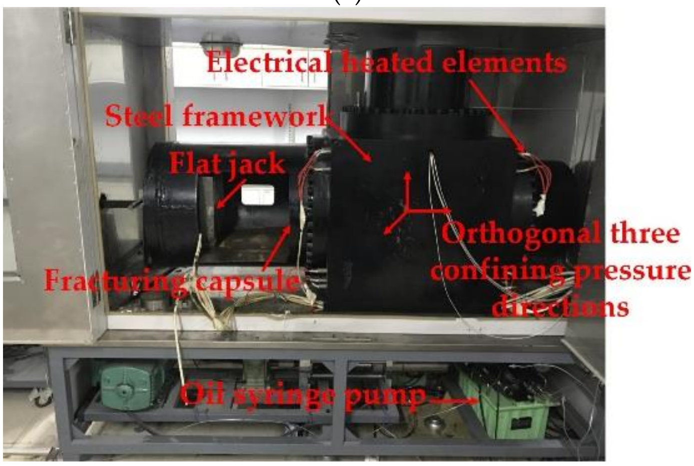


(b)


(c)

**Figure 4.** The true-triaxial hydraulic fracturing apparatus: (**a**) the water injection system; (**b**) the steel framework, confining pressure system, and the heating system; (**c**) the fracturing capsule.

The water injection system consists of four syringe pumps, they can provide a maximum injection flow rate of 30 mL/min, and a maximum pressure up to 80 MPa. The steel framework and confining pressure system consists of a steel framework with minimum yield of 60 MPa, three square flat jacks and a control panel. The steel framework contains a fracturing capsule that could support a cubical rock sample no larger than 300 × 300 × 300 mm. The three square flat jacks are placed in the three directions of the fracturing capsule and could provide three independent stresses, the independent orthogonal stresses applied on the three directions are used to simulate the underground in-situ stresses when a rock sample is buried underground. The flat jacks directly load and contact with sample faces, the framework is used as the opposing reaction faces, and hence flat jack and framework are the active and passive face, respectively. Each flat jack is pressurized and load through an independent oil syringe pump, the pressure data is recorded by the computer system. The face of square flat jack is 5 mm smaller than the sample face on each side. This will ensure that the adjacent square flat jacks will not come into contact to prevent jamming in loading stage. The heating system can heat the sample to a maximum temperature of 150 °C. The heating system is provided by three electrical heated elements. Two are installed on the top of the internal surface of the frame, and one is installed on the bottom of the fracturing capsule. Two 1200 W heating elements installed on the frame body can give approximately 2400 W heating capacity. Two additional 1000 W heating element is installed on two side of framework. The heating system allows different temperature set-points for the insulation can and fracturing capsule. The insulation can enclose the whole framework during heated, it will improve safety and reduce thermal losses. The computer monitor system could monitor the hydraulic fracturing pressure, rock sample temperature and control the injection flow rate.

### *2.4. Experimental Set-Up*

This study aims to investigate the influence of the fracturing fluid flow rate on the fracture initiation, propagation geometry and permeability. Therefore, to ensure the stress regime will not influence the tests' results, the same principal stress was applied on all specimens. Consequently, a maximum principal stress ($\sigma_1$) of 12 MPa, an intermediate principal stress ($\sigma_2$) of 8 MPa, and a minimum principal stress ($\sigma_3$) of 4 MPa were exerted on all samples. Such stresses will represent the in-situ stress regime of $\sigma_1 > \sigma_2 > \sigma_3$.

When hydraulic fracturing, the water fracturing pressure is usually between 10 and 40 MPa. The key to the success of this experiment is to ensure the sealing of the water outlet hole (Figure 5a) on the flat jack and the water inlet of the injection tube. Otherwise, the water will flow out from the connection of the flat jack and the injection tube without fracturing the rock sample. As the water outlet on the flat jack is slightly larger than the water inlet of the injection tube, to prevent fluid leakage, a rubber ring (Figure 5b) is sleeved on the injection tube head and the Poly Tetra Fluoroethylene (PTFE) sealing tape (Figure 5b) was wrapped on the outside of the rubber ring.


(**a**) (**b**)

**Figure 5.** (**a**) The water outlet hole in the flat jack; (**b**) the water inlet on the rock, the black color ring is the rubber ring, and the white color wrapped the black color is the PTFE sealing tape.

In an ideal circumstance, hydraulic fracture should propagate perpendicular to the minimum principle stress which is the preferred fracture direction (PFD) [40]. Hence, each testing sample was placed in the fracturing capsule in a way that the wellbore axis was along the intermediate principal stress direction, and, the maximum and the minimum principal stress were set perpendicular to the wellbore axis. This method makes it easy to observe relationship among the fractures, the maximum and the minimum principal stress when the sample is cut in half perpendicular to the wellbore axis, Figure 6 shows the sample was installed in the fracturing capsule.

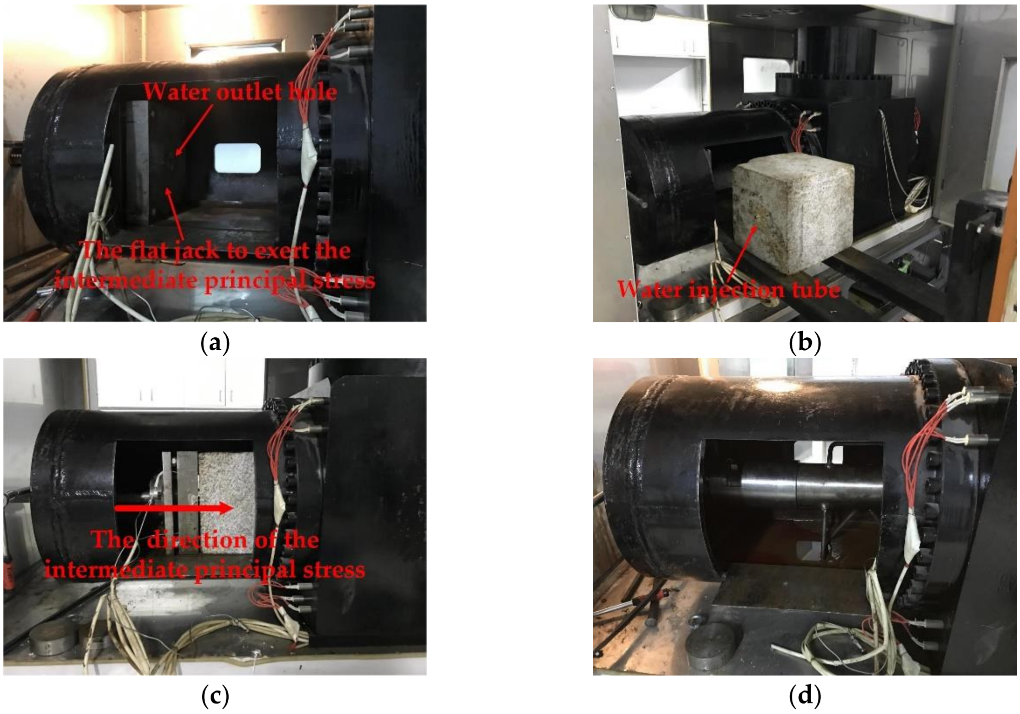


**Figure 6.** A rock sample is put into the fracturing capsule: (**a**) The rock sample is not put into the capsule; (**b**) A rock sample was putting in to the fracturing capsule; (**c**) The rock sample is push into the fracturing capsule; and (**d**) Three directions confining stresses are applied.

It should be noteworthy that the triaxial principal stresses were applied in four steps. Firstly, the intermediate principal stress was increased to the minimum principal stress. This procedure would ensure the exposed part of the injection tube is insert into the water outlet hole on the flat jack. Then the other two stresses were applied to the minimum principal stress magnitude. At this time, the minimum stress syringe pump was set on a constant value. Next, the intermediate and the maximum stress were applied to the intermediate principal stress regime, and their corresponding pumps were set as the intermediate stress. At last stage, the maximum principal stress was applied to maximum stress and then the maximum stress syringe pump was set as constant. This stress load method was applied to all experiments.

### *2.5. Experimental Process*

Samples were put into a cubic capsule and the triaxial confining stresses were applied. The triaxial confining pressure represents the in-situ stress. It is important to wrap the water in the wellbore after drilling and install the sample properly for the experiment success. Distilled water as the fracturing fluid was used to examine the effects of fracturing fluid flow rate on the fracturing pressures and propagation geometry. Six granite samples were test under 150 °C, and for each test the fluid is injected under a constant flow rate, the flow rate in different experiment ranges from 5 to 30 mL/min. During the testing, fracturing pressures were recorded.

Experimental procedures: (1) The apparatus was checked; (2) The rock sample was placed into the fracturing capsule; (3) Oil was pumped into syringe pump, triaxial stresses were applied to the rock sample at a rate of 0.3 MPa/s, and to ensure the rock was not damaged before the fracturing fluid was injected, the three principle pressure data was displayed on the computer monitor in real-time; (4) The heating system was turned on to heat the rock sample, the rock sample was heated to 150 °C and the temperature is maintained for 5 hours to ensure that the whole rock has reached the target temperature; (5) After the rock temperature was stabilized, through the water injection syringe pumps, water was injected via the tube for fracturing, the injection flow rate was set as constant in each test, six injection flow rate were chosen (5, 10, 15, 20, 25, and 30 mL/min); (6) When a large amount of water flowed out of the fracturing capsule, the fracturing pressure was not change and reached an equilibrium state, we considered hydraulic fracturing was completed, water injecting syringe pump was turn off; (7) The triaxial stresses were released, the stress release process was the same as the applying process, the maximum principal pressure was decreased to the intermediate principal pressure, next the intermediate and the maximum pressure were decreased to the minimum principal pressure, last the three principal pressures were released to zero; (8) The rock sample was taken out from the fracturing capsule, the fractures were observed and recorded immediately, the condition of water flowing out from the fractures could be clearly seen, water flowed out of rock sample along the fractures; (9) The rock specimens were cut in half to observe fractures; (10) Fractures were marked by a marker pen, and photographs were taken for recording; and (11) The experiment data is analyzed.

### *2.6. Experimental Uncertainty*

The uncertainties were mainly caused by measuring accuracy of hydraulic pressure, injection flow rate and fracture size. The fracture length was measured by Vernier calipers with accuracy of ±0.02 mm. The hydraulic pressure is measured with ±0.1 % accuracy in a range of 80 MPa. The injection flow rates is measured with ±1 % accuracy in a range of 30 mL/min.

## 3. Results

Hydraulic fracturing experiments were conducted on six 300 × 300 × 300 mm cubic granite samples. These experiments involved the injection flow rates from 5 to 30 mL/min with heated temperature of 150 °C (The 150 °C is the maximum temperature the heating system could provide). A confining pressure regime was maintained in the whole testing process on all six samples, where $\sigma_1$ = 12 MPa, $\sigma_2$ = 8 MPa, and $\sigma_3$ = 4 MPa. The wellbore, adhesive and perforation were processed with repeatability to make sure that each sample would be near identical when the fracturing stress applied by the high-pressure fracturing fluid. The triaxial confining stresses were applied slowly with significant level of care and caution to prevent stressing fractures in the loading process. This makes it possible to control most of the variables present in the experiment and to accurately monitor and study the effect of changing the flow rate of fracturing fluid injection Table 3 presents the fracturing parameters of the experiments.

**Table 3.** Fracturing experimental parameters and results.

| Test No. | Injection Flow Rate (mL/min) | Initiation Pressure (MPa) | Breakdown (Maximum) Pressure (MPa) | Post-Fracturing Pressure (MPa) | Propagation Time (s) |
|---|---|---|---|---|---|
| 1 | 5 | 21.06 | 22.12 | 11.20 | 613 |
| 2 | 10 | 22.95 | 24.68 | 12.69 | 498 |
| 3 | 15 | 25.61 | 27.65 | 11.27 | 447 |
| 4 | 20 | 27.91 | 30.06 | 9.97 | 343 |
| 5 | 25 | 28.71 | 34.10 | 7.68 | 220 |
| 6 | 30 | 32.52 | 36.01 | 3.11 | 88 |

At the end of each test, the sample was then taken out from the fracturing capsule after the triaxial confining stresses were released to atmospheric pressure. The fractures on the sample were photographed and marked (Figure 7a). Then the samples were carefully cut in half (Figure 7b). The fractures on each half were then photographed to analyze the fracture geometries.

(**a**) (**b**)

**Figure 7.** (**a**) The photo of the fractured rock sample, the black lines indicate fractures, red water flows out of the rock from these fractures and (**b**) the cut sample.

Figure 8a–f shows the fracturing pressure curves and pressurization rate of tests 1–6, where the hydraulic fracturing injection flow rates were 5, 10, 15, 20, 25, and 30 mL/min. The black curves represent the fracturing pressures. As Figure 8a–f show, all the pressure curves have similar shapes, a particular pressure–time curve could be divided into four main stages: initial pressure development stage, wellbore pressurization stage, fracturing stage, and post failure stage. During the initial pressure development stage, the fracturing fluid syringe pumped the water into the wellbore through pipeline. As the injection pump was the next room, the water injection pipeline was somewhat long, and this time interval lasted about 130–400 s and ended up when the wellbore was filled of water. At the end of this stage, the water was just filling the pipeline and injection tube. Very small pressure development was identified, and the pressure curve kept close to zero (almost horizontal) and unchanged. After the wellbore was completely filled, during the well-bore pressurization stage, continuously injecting water into the wellbore resulted in the rock around the wellbore bottom to be pressurized and the fracturing pressures started to quickly build up with an almost constant increase rate. Then in the fracturing stage, the fractures are initiated and propagated, new volume is created, the pressure reaches the maximum, which is also called breakdown pressure, and then has a large drop. In this stage, fractures were continuously induced by the high fracturing pressure, and new fluid is pressurized in to compensate the new fractured volume. Even though continuing to injection water, a large pressure drop was observed because of the large amount of new created volume which was not be absolutely compensated by the new injected water. The maximum pressure is 22.12, 24.68, 27.65, 30.06, 34.10, and 36.01 MPa when the injection flow rates were 5, 10, 15, 20, 25, and 30 mL/min, respectively. It was shown that the breakdown pressure increases with the increase of injection flow rate. The fracturing stage lasted a few seconds, when the fracture tip reached the sample boundary, the fracturing stage reaches to the last stage, the post-failure stage, and the fluid flows out of the sample. Even though water is continuously injected into rock sample, the pump pressure did not change. This means that the injection pressure was now equal to the water flowing frictional pressure loss along the created fractures, even if new injected water entered into rock body and no fracture would be created. The injection pressures do not change with time and the wellbore pressures are stable, water flowed out of the rock sample along the fractures into the fracturing capsule.

The red curve represents the pressurization rate. It could help to analyze different stage during the fracture propagation. As shown in Figure 8a–f, a typical pressurization rate curve could obvious reflect different phase during fracture propagation. In the initial pressure development phase, as the water only filled the injection tube and the pressure was almost keep at zero, the pressure did not change at this phase and the pressurization rate was kept at zero. In the well-bore pressurization phase, fracturing fluid filled full of the well-bore and the pressure was applied to the rock mass around the wellbore bottom. As the injection flow rate was constant, the pressurization rate rose rapidly and then fluctuates near a constant value, this represents the pressure curve ascended approximately in a straight line at this phase. When entering the fracturing phase, the pressurization rate decreased rapidly until it became negative, which indicated that the injection pressure decreased dramatically in a non-linear form. It showed that the fractures propagated very fast, and the new pumped fracturing fluid could not fill full of the rapidly new formed fractures. In the last phase, the fracture tip hit the rock boundary, no new fracture was created, the fracturing fluid just flowed out of the rock along the formed fractures, the pressure did not change, and the pressurization rate gradually became zero.

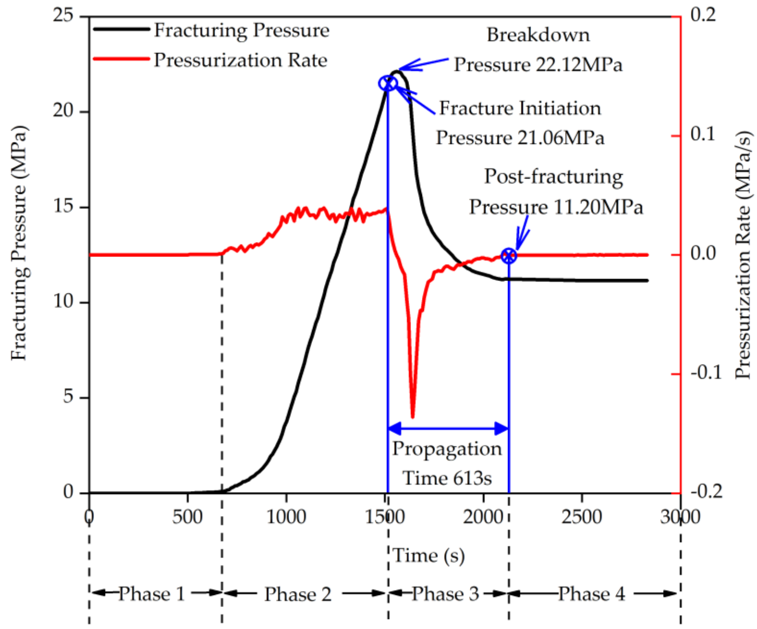


(**a**)

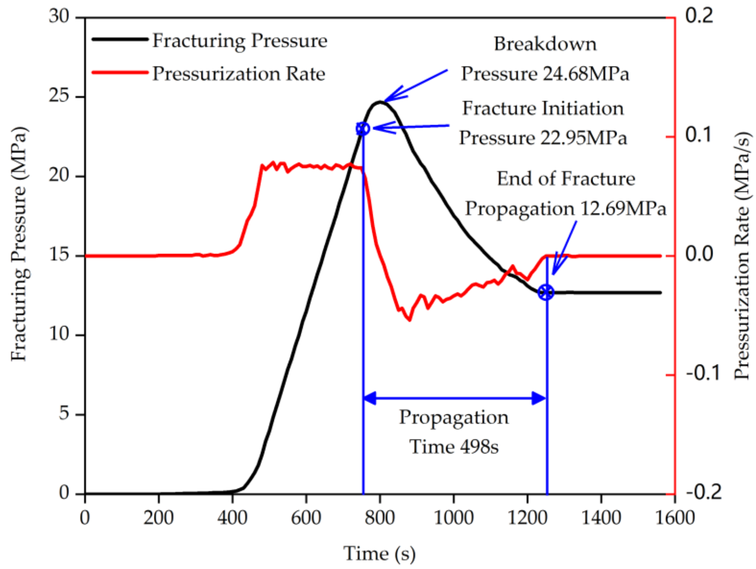


(**b**)

**Figure 8.** *Cont.*

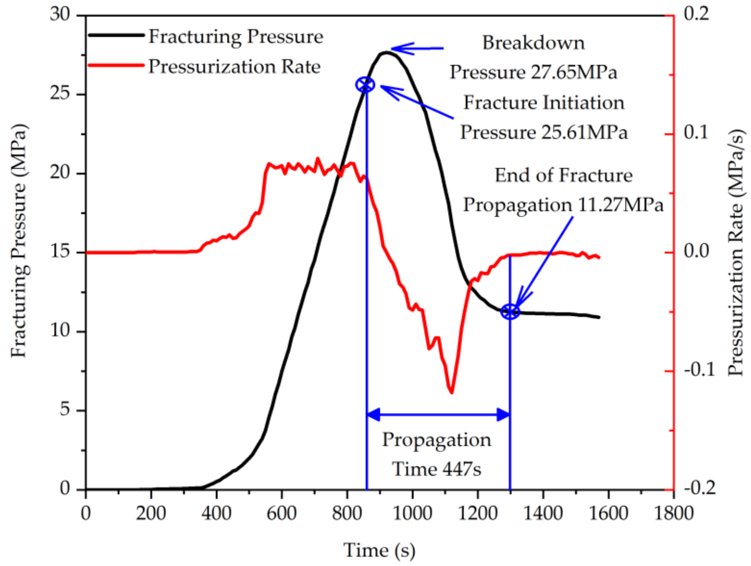

Fracturing Pressure
Pressurization Rate
Breakdown Pressure 27.65MPa
Fracture Initiation Pressure 25.61MPa
End of Fracture Propagation 11.27MPa
Propagation Time 447s
Fracturing Pressure (MPa)
Pressurization Rate (MPa/s)
Time (s)


(**c**)

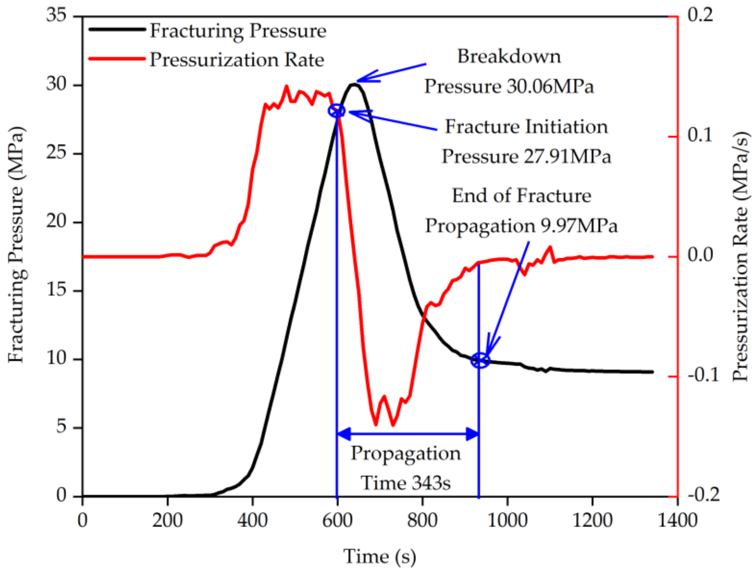

Fracturing Pressure
Pressurization Rate
Breakdown Pressure 30.06MPa
Fracture Initiation Pressure 27.91MPa
End of Fracture Propagation 9.97MPa
Propagation Time 343s
Fracturing Pressure (MPa)
Pressurization Rate (MPa/s)
Time (s)


(**d**)

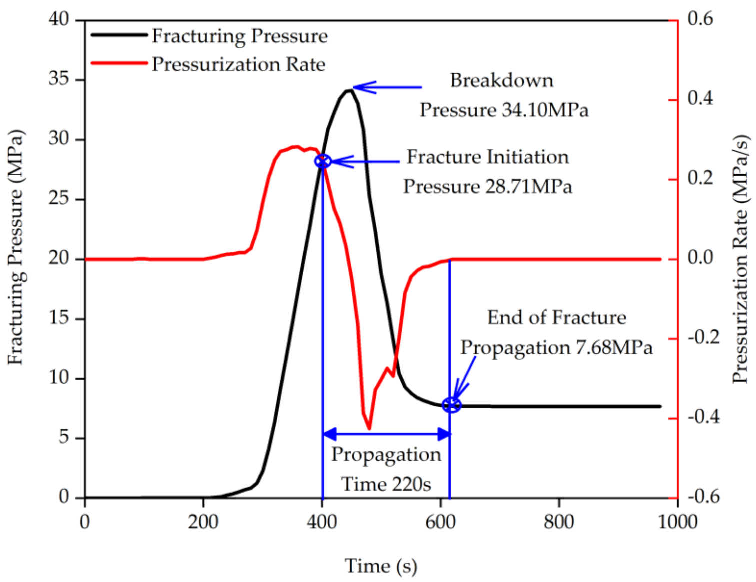

Fracturing Pressure
Pressurization Rate
Breakdown Pressure 34.10MPa
Fracture Initiation Pressure 28.71MPa
End of Fracture Propagation 7.68MPa
Propagation Time 220s
Fracturing Pressure (MPa)
Pressurization Rate (MPa/s)
Time (s)


(**e**)

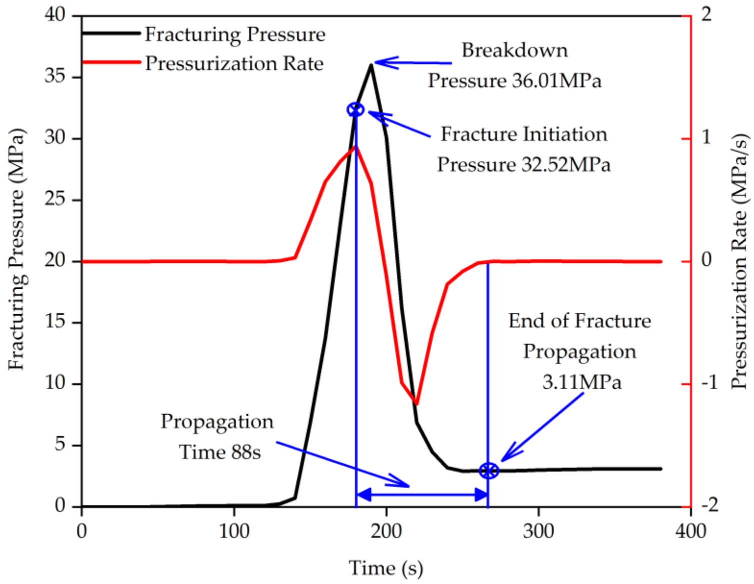


**(f)**

**Figure 8.** The fracturing pressure–time curves and pressuring rate–time curves: (**a**)–(**f**) are the hydraulic pressure curves and pressure rate curves when the injection flow rate is 5, 10, 15, 20, 25, and 30 mL/min, respectively.

Figure 8a illustrates the hydraulic pressure and pressure rate evolution with time of experiment 1, and the injection flow rate is 5 mL/min, stages 1–4 are respectively: (1) the initial pressure development stage, (2) the well-bore pressurization stage, (3) fracturing stage, and (4) post-failure stage. Figure 8b shows the curves of the injection flow rate of 10 mL/min. Figure 8c illustrates the curves of the injection flow rate of 15 mL/min. Figure 8d illustrates the curves of the injection flow rate of 20 mL/min. Figure 8e illustrates the curves of the injection flow rate of 25 mL/min. Figure 8f illustrates the curves of the injection flow rate of 30 mL/min. As shown in Figure 8 a–f, the shape of the pressure–time curves and pressure rate–time curves are with four stages.

## 4. Discussion

### *4.1. The Effect of Flow Rate on the Fracture Initiation Pressure*

Usually we call the maximum pressure as the breakdown pressure and it seems that the rock sample is fractured and fails when the pressure reaches the maximum. However, the rock around the wellbore bottom already begins to be fractured before the maximum pressure [41]. To properly make sure the fracturing initiation pressure is helpful to analyze the rock properties, such as failure stress, tensile stress, and shear stress in real field hydraulic fracturing. Accurate estimation of fracturing initiation pressure is also important for the effective and efficient designing of hydraulic fracture schemes. It will directly influence hydraulic fracturing method and difficulty in field-scale operations [42].

To find out the time of fracturing initiation, we firstly analyze the hydraulic fracturing process. When the wellbore is full of water, the pressure will rise quickly. When enough fluid is pressurized, a fracture initiates from the bottom of the wellbore, and some new volume is induced. The pressurized fracturing water near the wellbore bottom expands to fill the new initiated flaw volume, and thus reducing the wellbore pressure. At the same time, the pressurized water will naturally, via syringe, quickly flow into the wellbore to compensate this pressure drops. As the new pressurized water volume is larger than the new induce crack volume. This may induce higher pressure in the wellbore, but wellbore pressure would not increase obviously. As a result, we can find that the highest fracturing pressure always lasts for a while from the fracturing pressure recording curve. This phenomenon will definitely cause the decrease of the pressurization rate. Then the initiated fracture will propagate towards the boundary of the sample and more volume is developed. When the pressurized fluid cannot compensate the new volume. The pressure curve declines. When the fractures reach the sample's boundary and the fluid flows out of the sample, the pressure becomes stable. The pressure does not fluctuate and the pressurization rate become zero.

Based on the analysis of fracturing process, we find that the pressurization rate could be used to indicate the fracturing initiation, fracturing termination, and propagation time. In Figure 8a–f, the red curves are the pressurization rate curves. When the wellbore is not full of fracturing fluid, the pressure keeps at zero and the pressurization rate is also kept at zero. Then the pressurization rate rapidly rises and usually fluctuates in a constant vale for a while at the top of the curve. In this period, fluid is full of the wellbore and still pressurized into the wellbore, no fracture is initiated. As the flow rate is constant, the pressure rises approximately linearly with time, and the pressurization rate is almost constant with little fluctuations. The beginning of a quick decline in the pressurization rate curve could be considered as evidence of the fracture initiation point. As the rock in the wellbore bottom could not withstand the high pressure, the fracture initiates, micro cracks are induced, thus, the wellbore pressure increase rate reduces. This is the reason that the new pressurized water expands from the wellbore to fill the new induced fracture volume and the new pressurized fluid cannot absolutely compensate the pressure reduction, consequently the pressurization rate decreases. When the fracture tip is going to hit the sample boundary, the pressure is almost equal to fluid friction loss pressure along the pathway, the pressurization rate rises and gradually becomes zero.

Based on the above analysis, the fracture initiation pressure could be regarded as the time when the pressurization rate begins to rapidly decrease, at which the fracturing pressure has not yet reached the maximum value (see Figure 8a–f). We can find that, from Figure 8a–f and Table 3, with the flow rate increase, the initiation pressure also increases. Hence, the injection flow rate influences the initiation pressure in hydraulic fracturing.

Figure 9 shows the initiation pressure under different injection flow rates in different tests, the initiation pressure is approximately positive linearly increasing with the injection flow rate. For instance, the initiation pressure ascends from 21.06 to 32.52 MPa as the injection flow rate is increased from 5 to 30 mL/min, the initiation pressure increases 54.42%. And the coefficient of determination was 0.9808.

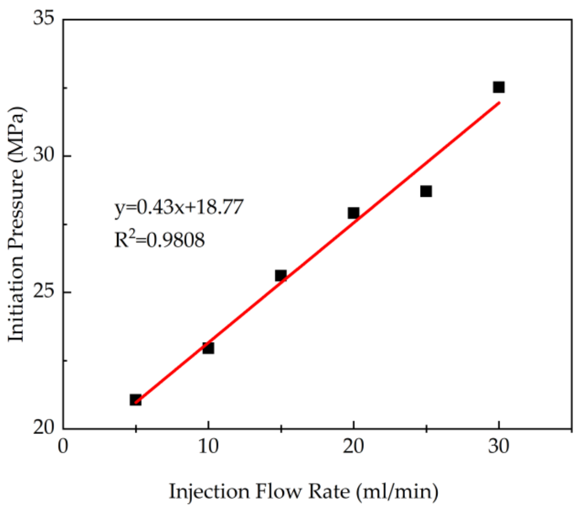


**Figure 9.** Influence of injection flow rate on the initiation pressure.

### *4.2. The Effect of Flow Rate on the Fracture Propagation Time*

The measurement accuracy of hydraulic fracturing pressure depends on the accurate interpretation of the fluid pressure–time curves [43]. The fracture propagation time is a crucial parameter to estimate fracture extension range in field scale hydraulic fracturing [44]. In development process of oil, gas, and geothermal fields, the time of hydraulic fracturing will also directly influence the number and magnitude of the induced earthquakes [45].

In laboratorial hydraulic fracturing tests, the fracture propagation time is usually the time interval that it takes from the fracture initiation until it grows all the way to the boundary of the experimental sample from the wellbore bottom. After a fracture is triggered, the fracture grows, more and more new volume will be induced, and the wellbore pressure decline rate will accelerate. This is shown in Figure 8, where wellbore pressurization rated (red curves) are decreasing after the fracture initiation points. It could be considered to be the beginning of the fracture propagation. When the fracture reaches the sample boundaries, the fluid begins to flow out into fracturing capsule from the fractures. The pressure in the wellbore is now equal to frictional pressure that the fracturing fluid loses along the fracture pathway. As the fracturing pressure is stable and does not change with time and the pressurization rate becomes zero without fluctuation. This is the time point (see Figure 8) that could be practically considered as the fracture propagation ending, and the remaining the pressure–time data represent the new injected water flowing via the fracture pathway. Through the pressurization rate curve, we can easily determine the propagation time. The fracture propagation time (see Figure 8) could be considered as the time interval between the fracture initiation and the fracture end.

The propagation time of a granite specimen with different injection flow rates is shown in Figure 10. As shown in Figure 10, with the increase of injection flow rate, the propagation time has a linear decrease trend. The propagation time decreases from 613 to 88 s when the injection flow rate increases from 5 to 30 mL/min, the propagation time decreases 85.64%. At the same time, the propagation times are linearly fitted with the determination coefficient of 0.9851. This relationship represents that with the increasing of injection flow rate, more fluid is pumped into the wellbore in the same time interval, more new volume is created, the fracture propagation rate also increases, and the fracture propagation time decreases.

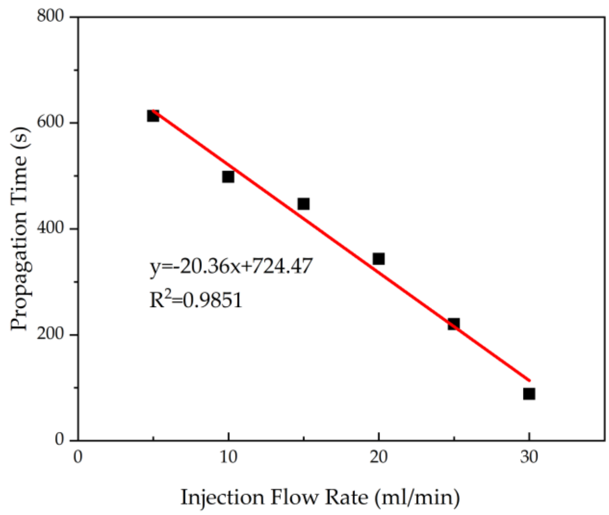


**Figure 10.** Influence of injection flow rate on the propagation time.

Usually, induced earthquakes are accompanied with a whole hydraulic fracturing process, a longer fracture propagation time always means that more earthquakes are triggered [45]. In an in-situ project, a traditional view is that the maximum induced earthquake magnitudes are only related to the volume of injected fluid [46]. Therefore, to get a good fracture network and avoid a dangerous earthquake, a small injection flow rate with a long propagation is always adopted in field-scale operation over recent years [47,48]. Whereas, this method also could cause a large earthquake, for example, hydraulic fracturing of the Pohang hydraulic fracturing project almost lasted several months over two years, a $M_w$ 5.5 earthquake was caused, this earthquake injured about 70 people and induced extensive damage to the Pohang city [49]. Since the seismographs were firstly installed in 1905, this induced earthquake was the most damaging, and the magnitude is second-largest in South Korea [50]. As a result, it is necessary for hydraulic fracturing to choose a reasonable fracturing propagation time.

### *4.3. The Effect of Flow Rate on the Post-Fracturing Pressure*

The post-fracturing pressure is the almost constant pressure with time after the fracture reaches the rock boundary, when the fracture length does not increase. This time point is illustrated in Figure 8a, after this time point, the pressure–time data recorded is just showing the process that water flows via the created fracture to rock boundary. The pressure in the wellbore remains almost constant. It is noteworthy that the post-fracturing pressure behavior is very similar to the fluid injection pressure during the heating extraction stage or petroleum extraction stage after hydraulic fracture in the field for an in-situ project. This injection pressure (post-fracturing pressure) is based on the concept that when constant viscous fluid in isothermal reservoir condition flows through a constant length fracture pathway, the frictional pressure loss along the pathway does not change with time. In an in-situ project, the requirement for hydraulic fracturing technology is very high. If the fractures are too developed (indicating a low post-fracturing pressure), the water flows too fast in the fractures, the heat exchange time between the rock mass and water is short, the heat transfer is insufficient, and the water temperature at the water outlet well is low. The thermal energy cannot be well exploited. If few fractures propagate insufficiently or the fracture channel is narrow (indicating a high post-fracturing pressure), the water cannot flow through the inlet wellbore to the outlet wellbore well, it may result in serious water loss or less water could flow out of the outlet wellhead. We will not yet achieve the purpose of thermal energy exploitation. Therefore, in hydraulic fracturing, we need properly propagated fractures, water not only can flow well in the fracture, but also can have a good heat transfer with rock thermal reservoir along fractures. However, the fractures cannot be directly observed after hydraulic fracturing in field-scale operation, and we need to find other methodologies to interpret the fracturing pressures.

In laboratorial hydraulic fracturing experiments, the post-fracturing pressure is the frictional pressure loss when fluid flows through the whole fracture system. It is in accordance with the injection pressure during the in-field heat extraction phase and could directly reflect the fracture condition and it is an important parameter to determine the heat extraction efficiency and to evaluate the hydraulic fracturing results.

As the injection flow rates are different in tests, the post-fracturing pressures could not be used for analysis directly. To test the fracture network and contrast the post-fracturing pressures in different tests, the flow rate is change to 5 mL/min at the end of each test. If injection flow rate was greater than the least flow rate, new fractures might be triggered for the samples whose flow rate (the flow rate in Table 3) was lower during hydraulic fracturing experiment stage. So, we choose the lowest flow rate when revising the post-fracturing pressures. Table 4 presents the post-fracturing pressures when the flow rates are changed to 5 mL/min, they are called the revised post-fracturing pressures. We can see that a higher injection flow rate during the experimental (hydraulic fracturing) phase, a lower revised post-fracturing pressure is caused.

**Table 4.** The revised post-fracturing pressures.

| Test No. | Injection Flow Rate during Hydraulic Fracturing (mL/min) | Post-Fracturing Pressure (MPa) | Revised Post-Fracturing Pressure (MPa) |
|---|---|---|---|
| 1 | 5 | 11.20 | 11.20 |
| 2 | 10 | 12.69 | 11.13 |
| 3 | 15 | 11.27 | 9.52 |
| 4 | 20 | 9.97 | 6.37 |
| 5 | 25 | 7.68 | 4.59 |
| 6 | 30 | 3.11 | 1.43 |

As shown in Figure 11, the revised post-fracturing pressure is linearly decreasing with the injection flow rate increasing. The revised post-fracturing pressure decreases from 11.2 to 1.43 MPa (a gradient of 87.23%) when flow rate increases from 5 to 30 mL/min. And after linearly fitted the revised post-fracturing pressure data, a coefficient of determination 0.9926 is achieved. We can see that a lower revised post-fracturing pressure corresponds to a lower injection flow rate after hydraulic fracturing, a higher revised post-fracturing pressure corresponds to a higher injection flow rate. It means a lower injection flow rate may cause a fracture network with less fractures and narrow channels for water flowing through, whereas a higher injection flow rate may lead a developed fracture network that water could easily flow through.

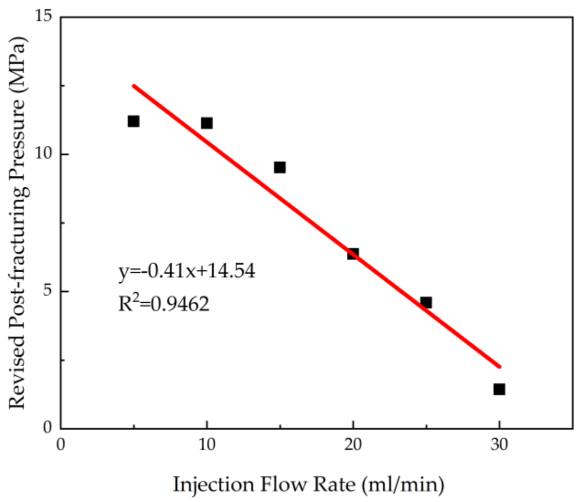


**Figure 11.** Influence of injection flow rate on the revised post-fracturing pressure.

The post-fracturing pressure is an effective parameter to estimate the fracture opening and leak off during hydraulic fracturing [43]. It also could help to analyze the fracture geometry, length, and smoothness, a lower post-fracturing pressure usually corresponds to a better-connected fracture network with longer and smoother fracture branches [51]. The post-fracturing pressure is an indispensable parameter when predicting the productivity of wells after hydraulic fracturing [52]. Therefore, it is necessary to correctly identify the post-fracturing pressure and find out its changing laws.

### *4.4. The Effect of Flow Rate on the Fracture Breakdown Pressure*

Usually, the fracture breakdown is defined as the time point when the pressure in wellbore reaches the maximum, this means that fracture breakdown typically occurs after the point of initiation [53–55]. The fracture-initiation pressure is the time point when a tiny defect near borehole begins to propagate and the breakdown pressure is usually larger than the fracture-initiation pressure [41,56]. In general, we need to distinguish the initiation pressure and breakdown pressure when considering the problem of fracture propagation.

The breakdown pressure always occurs after the initiation pressure when the fracture is just initiated and the new created volume cannot compensate the injected fluid. The breakdown process represents a situation that the water supply (the amount of water injected into the wellbore) is greater than the water demand (the water volume needed to propagate the fracture), the wellbore bottom pressure continues to rise. A higher pressure (breakdown pressure) will be caused.

The initiation pressure represents the pressure when the fracture begins being initiated. It is a parameter that could reflect the properties of the rock sample. The breakdown pressure is the maximum pressure value in the pressure curve and it could be used to help to design the fracturing scheme, select a fracturing pump, and estimate the fracture range in field operation [57]. Therefore, it is necessary to separately analyze the initiation pressure and the breakdown pressure, whether for laboratory research or field scale engineering.

Figure 12 shows the change trend of the breakdown pressure under influence injection flow rate increase. The breakdown pressure is almost positive linearly increasing with the increase of injection flow rate. The coefficient of determination is 0.9943 after linearly fit. The breakdown pressure increases from 22.12 to 36.01 MPa when the injection flow rate increases from 5 to 30 mL/min, the breakdown pressure increases 62.79%.

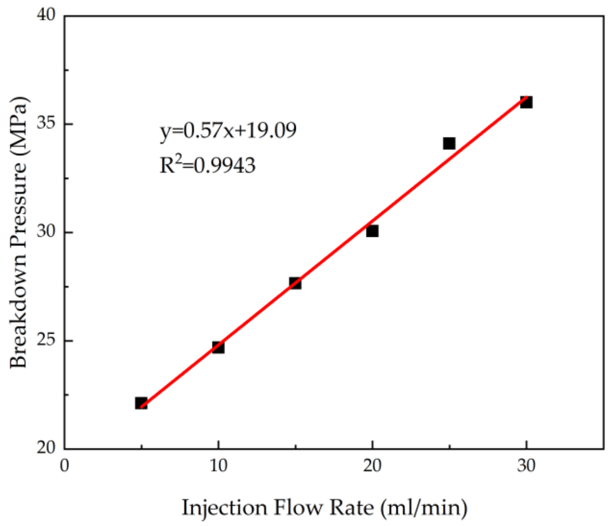


**Figure 12.** Influence of injection flow rate on the breakdown pressure.

The breakdown pressure is a very important parameter during the hydraulic fracturing process [11]. A previous study also showed that it could influence the fracture propagation patterns and fracture morphology [43,55,58]. The fracture approach mechanics of hydraulic fracturing was mainly determined by the breakdown pressure yet [59]. This parameter is widely used when analyzing the fracture behavior in a laboratorial test, numerical simulation, and in-situ project [15,43,56,60]. As a result, it is crucial to correctly determine the breakdown pressure and analyze its changing trend with the injection flow rate.

### *4.5. The Effect of Flow Rate on the Fracture Geometry*

The fracture geometry is of vital importance for the evaluation of hydraulic fracturing effect. The fracture length, height and morphology are important indexes to access the hydraulic fracturing results and investigate fracture extension patterns. To clearly observe these indexes of the fractures, the samples are cut in half at the wellbore bottom. Figure 13a–f show the fractures of test No. 1–6 samples. Table 5 presents the fracture total lengths.

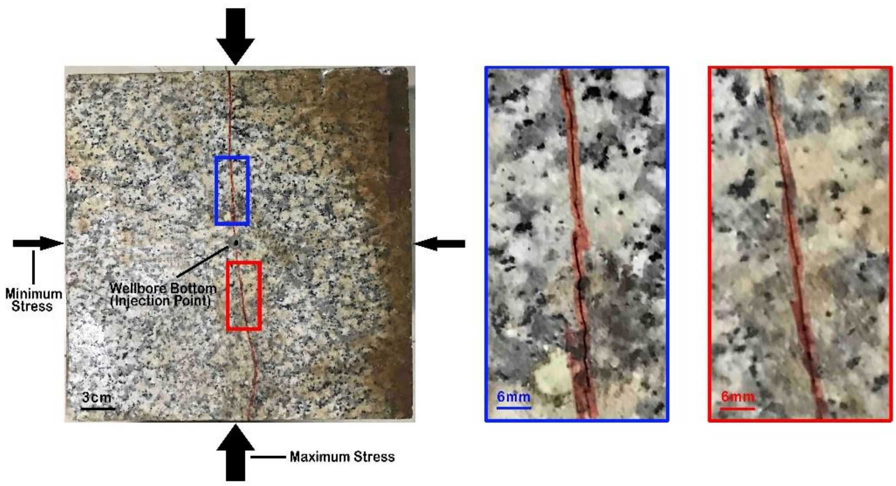


(**a**)

**Figure 13.** *Cont.*

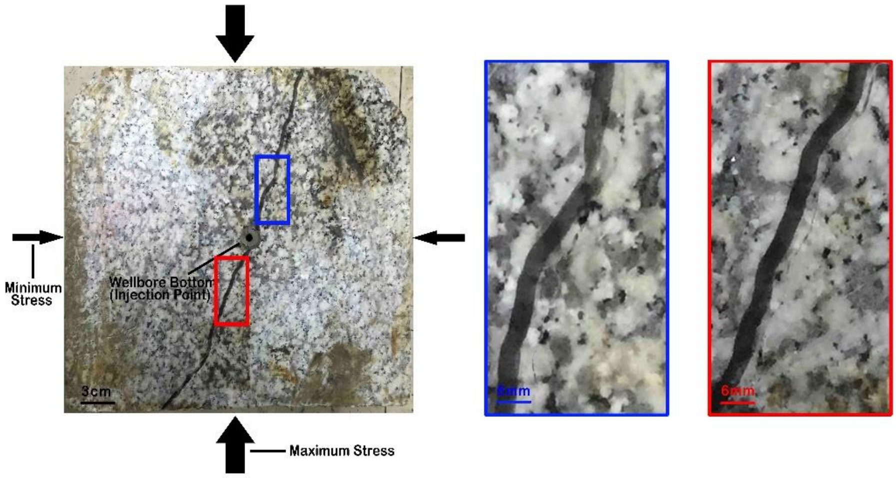


(**b**)

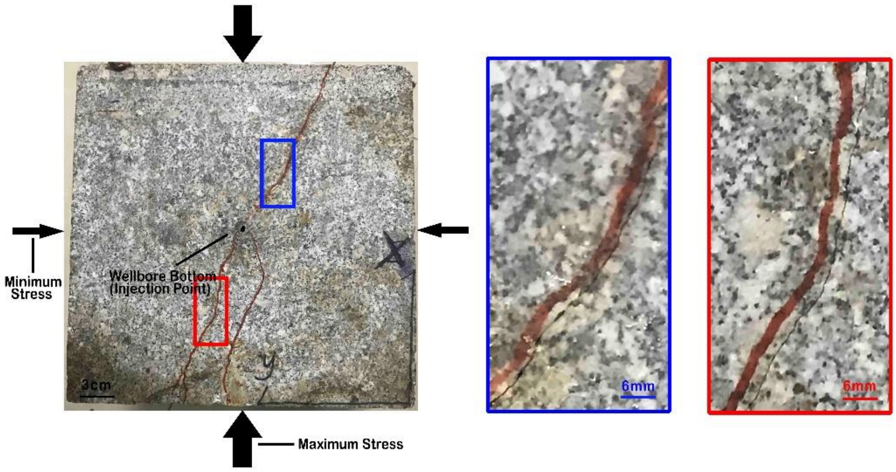


(**c**)

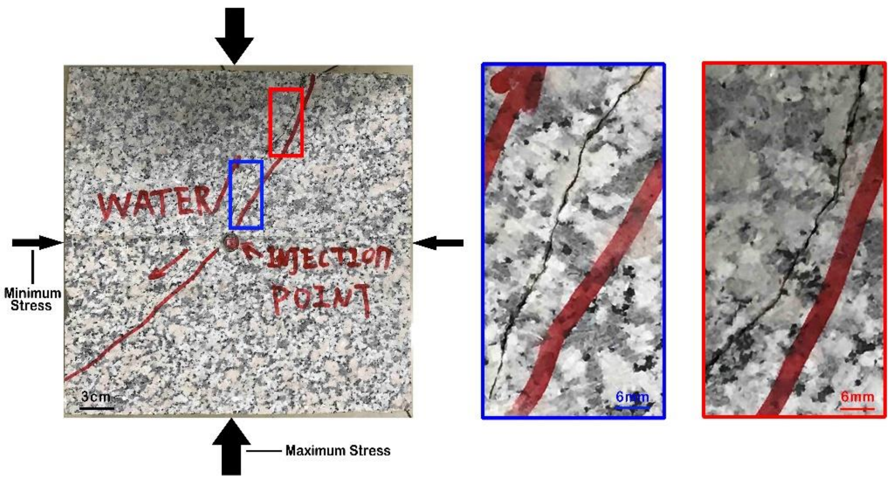


(**d**)

**Figure 13.** *Cont.*

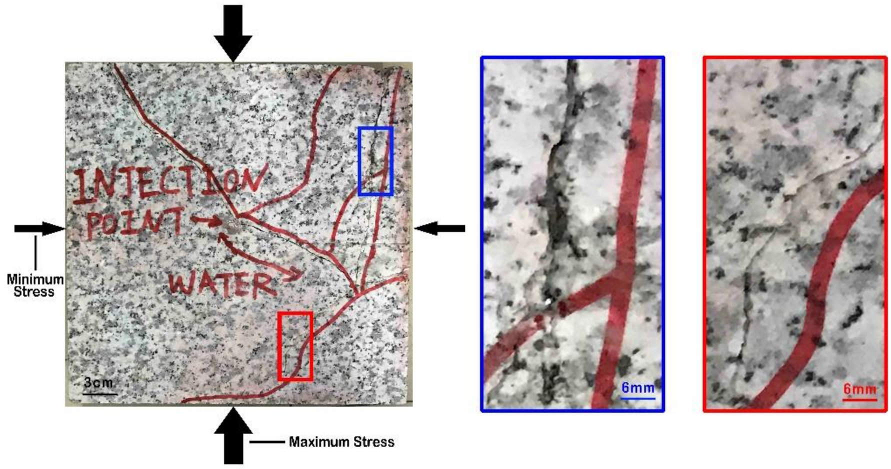


(e)

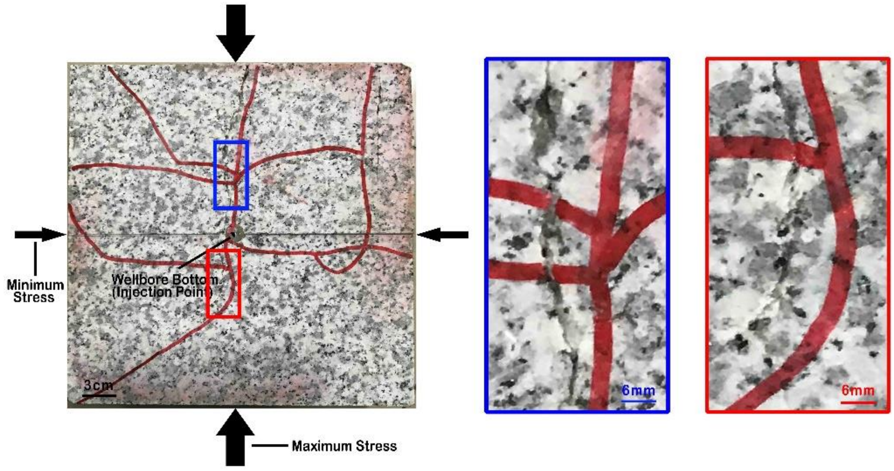


(f)

**Figure 13.** The fracture geometries of Tests 1–6: (**a**)–(**f**) are the fracture geometry photos after the rock samples were cut in half when the injection flow rate was respectively 5, 10, 15, 20, 25, and 30 mL/min, all the fractures were marked, the blue rectangles are enlarged by five times and displayed in the middle, the red rectangles are enlarged by five times, and displayed on the right side.

**Table 5.** The Fracture Total Length.

| Test No. | Injection Flow Rate (mL/min) | The Total Length of Fractures (mm) |
|---|---|---|
| 1 | 5 | 319 |
| 2 | 10 | 342 |
| 3 | 15 | 467 |
| 4 | 20 | 388 |
| 5 | 25 | 1089 |
| 6 | 30 | 1386 |

In Figure 13a, only a two-wing fracture is induced in the Preferred Fracture Direction (PFD), that is the maximum principle pressure axis direction, the direction of the fracture is almost perpendicular to the direction of the minimum stress. In Figure 13b, only a two-wing fracture is induced. The upward fracture and downward fracture have angles of about 15.4° and 19.2° with the PFD respectively, the propagation angles are small, and the fractures are considered along the PFD. In Figure 13c, a three wing fracture is induced. The upward fracture propagation angle is 30.0°, which is larger than the two downward ones (14.8° and 19.44°). As the angles are less than 45°, the angles are closer to the maximum stress axis, and the downward fracture in left propagates a short path then turns towards the

PFD. As a result their propagation directions could be considered to be along the maximum principle pressure direction. In Figure 13d, only a two-wing fracture is propagated. The fracture propagates downwards and upwards both in a curved way, and the upward fracture turns towards PFD in a distance away from the wellbore. The downward fracture could not be obviously observed towards to PFD. In Figure 13e, three wings are initiated from the wellbore. The wing that propagates to the upper left has an angle of 34.3° with respect to PFD. The two wings that propagate to right almost against the PFD near the wellbore. Then the upper right one changed its direction towards the PFD. The lower left one propagates into three branches away from the wellbore, and two of them develop towards the PFD and merge upward into one fracture. The downward branch propagates along the PFD at first, and then develops against the maximum stress at the lower edge of sample. In Figure 13f, this test exhibited a multiple fracturing distribution, a fracture system with three wings are initiated from the wellbore. The upward wing propagates almost along the PFD. The upward one is the widest fracture and could be considered as the main hydraulic fracture. However, its three branches are almost against the PFD. The left downward wing is initiated along the PDF and then grows in a curved path to the lower left, its only branch propagates against the PFD. The right downward wing is initiated against the PFD at first and then its branch propagates along the PFD.

It was expected that a fracture propagation direction would be vertical along the PFD, perpendicular to the minimum principle stress. However, only the fracture in Test 1 (Figure 13a) propagated almost along the PFD, and most of the others were initiated in an angle respect to the PFD. As it still can be seen from Figure 13, fracture propagation in hydraulic fracturing is influenced by triaxial principal stresses (crustal stress in field). Although, sometimes the fractures are not initiated along the PFD near the wellbore, the fractures will gradually turn to PFD in curved paths as the fractures grow towards the boundaries of the samples. At last, the fracture propagate direction is the PFD. The reason is that the actual stress state near the wellbore zone is very complex. The initiation of hydraulic fracture is controlled by the in-situ stress, the wellbore, the wellbore internal pressure, the pore pressure, the rock stress condition, the rock anisotropy, and other mechanisms [54]. As a result, the fractures may be initiated not along the PFD at first. Once the fracture has some length, fracture propagation rate is stable, the fracture tip moves far away from the wellbore and stress complex area, the fracture goes into a less-stressed region, and then the fracture propagation will be controlled by the triaxial stresses and along the PFD, as the injection pressure is less than the breakdown pressure in this time, this means that less pressure is needed for the fracture propagation.

We could also see that in Tests 4, 5, and 6, some fracture branches still did not approach the PFD when they reached the rock boundary, and even parts of them were perpendicular to the PFD. As shown in Figure 13d–f, some of the main fractures, that propagated from the wellbore, could not be seen to turn towards the PFD when the fracture tips hit boundary. Fan and Hannes et al. [35] performed a series of studies, and showed that with the increase of injection flow rate, the balance between fracture propagation and fluid injection could be broken, the fracture propagation would become unstable and fluctuated, and it meant that the fracture propagation pathway might be unpredictable. And sometimes, in the area around the wellbore, the fracture propagation would not obey the PFD law. This was in accordance with our experiment results. Higher injection flow rate meant higher pump pressure and more energy available for rock failure near the injection wellbore. More energy was introduced into the rock, the chances of creating a complicated fracture network were increased [61]. The reason was that, when a lot of water was pumped into the wellbore in a short time, a high-pressure environment was formed rapidly at the bottom of the wellbore, this would lead the fracturing process to be similar to an explosion process, the fractures propagated rapidly from the wellbore to the rock boundary, and the hydraulic fracturing time was very short. As the energy and pressure were released rapidly, this kind of "exploded" fracture propagation pattern always triggered new tension fractures, and as a result, the fractures might not propagate along the PFD. Whereas, when the injection flow rate was low, the fracture propagation rate was low and the fracture tended to be shearing ones, shear fracturing always propagated along the weak points among the rock mineral particles approaching to the PFD and this process was controlled by the principal stresses [26]. Usually, in high injection flow rate, the "exploded" phenomenon only influenced the rock mass near the wellbore, when the fractures propagated far away enough, the propagation turned to the PFD again. But in our tests, the side length of the rock sample was only 300 mm, it may be still in the influence of the "exploded", so the fractures propagating towards the PFD was not obviously observed.

The description for the hydraulic fracture geometry was very important in the in-situ operation. A more complex and wider fracture might result in lesser frictional resistance and a higher permeability, the fluid flowed through the fractures would be more easily with less resistance, and as a result, in field-scale operations, the heat extraction time from rock would be short, the heat extraction efficiency would be low. On the other hand, fluid would suffer higher frictional pressures when flowing through a single narrow fracture. The flow rate was low and the heat extraction between fluid and rock was sufficient, whereas the total amount of fluid flowing through the fractures would also be low. As a result, the amount of the extracted heat was still low. So, an appropriate fracture geometry was vital for an in-situ project.

Analyzing fracture morphology after hydraulic fracturing would demonstrate how the injection flow rate could influence the fracture geometry. To compare and observe the fractures widths of different tests. We chose two parts to enlarge five times in the fracture photo of each test. In Figure 13, with the increase of the flow rate, the fracture generally became wider. Figure 14 showed the total length of the fractures varied with respect to injection flow rate. Generally speaking, the total length of fractures increased with the increase of flow rate. However, we could see that the total length of the fractures in Test 4 was less than that in Test 3. Combined with Figure 13, from the enlarged fractures photos, we could see that the fractures of Test 4 were wider, and the corresponding revised post-fracturing pressure in Table 4 was lower yet, it meant that the frictional resistance in Test 4 was lower than that in Test 3 when the fluid flowed through the fracture system, so it could be considered that it did not violate the flow rate-post fracturing pressure law. As a result, we could get that a higher flow rate led to higher initiation and breakdown pressures, wider fractures, and a more complex fracture system. This resulted in a higher connectivity of the fractures and a lower friction resistance for fluid flowing. The revised post-fracturing pressure in Table 4 was in accordance with this conclusion.

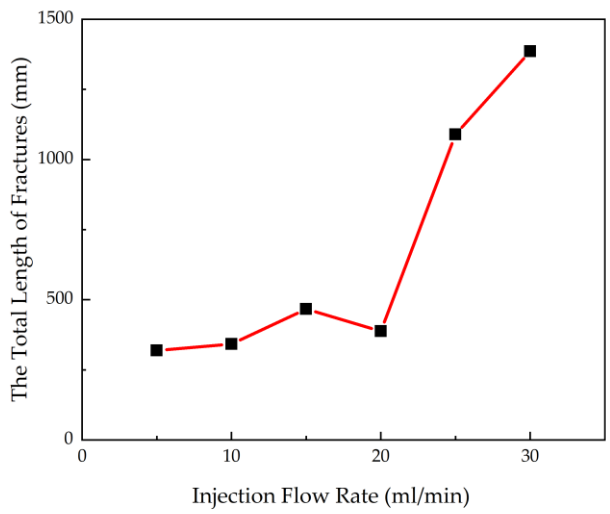


**Figure 14.** Influence of injection flow rate on the fracture length.

When the injection flow rate was increased from 5 to 20 mL/min, the total length of fractures increased, but the increase trend, as shown in Figure 14, was not obvious. When the injection flow rates were increased to 25 and 30 mL/min, the fractures total lengths had notable increase. Combined with Figure 13, the fractures in Tests 1, 2, 3, and 4 (injection flow rate from 5 to 20 mL/min) formed a two-wing or a three-wing fracture, a fractured network in these tests was not induced. As a result, the increase of injection flow rate only increased the fractures width, but not in the fracture length. This meant the fractures in Tests 1–4 should be mainly shear fractures. When the injection flow rate was increased to 25 mL/min (Test 5) and 30 mL/min (Test 6), the "exploded" fracturing mode was trigger, the fractures were mainly tension fractures. Fracture networks formed in the both two test and hence the fracture lengths had obvious increase. It showed that when the injection flow rate was low, the shear fractures were induced, and the hydraulic fracturing usually formed a main fracture without branches. When the injection flow rate was high enough, the tension fractures could be trigged, the hydraulic fracturing could form a fracture network.

### 4.6. The Mean Injection Power

Figure 14 recognizes the relationship between the injection flow rate and fracture total length, although by increasing the injection flow rate, a longer fracture length is induced, the mathematical relationship between the two parameters were not gotten from Figure 14.

To analyze the reason that injection flow rate could influence the geometry, width, and complexity of fractures. A new parameter called Mean Fracturing Power ($\overline{P}_I$) is put forward. Each test has a specific flow rate (Q), the fracturing pressure (P) varies as a function of time (t). In view the injection flow rate unit ($m^3$/s), hydraulic fracturing pressure unit (N/$m^2$), and time unit (s), it could be realized that the unit of the product of fracturing pressure, injection flow rate, and time will be N·m. This means that this product represents the energy that supplies for hydraulic fracturing. Hence, the $\overline{P}_I$ is defined as:

$$\overline{P}_I = \frac{\int_0^T Q \cdot P dt}{T}, \tag{1}$$

where $T$ is the fracture propagation time. The unit of $\overline{P}_I$ is power (W). Table 6 shows the Mean Fracturing Power of Test No. 1–6.

**Table 6.** Mean Fracturing Power.

| Test No. | Injection Flow Rate (mL/min) | Mean Fracturing Power (mW) | The Total Length of Fractures (mm) |
|---|---|---|---|
| 1 | 5 | 67.86 | 319 |
| 2 | 10 | 125.23 | 342 |
| 3 | 15 | 202.93 | 467 |
| 4 | 20 | 316.50 | 388 |
| 5 | 25 | 489.32 | 1089 |
| 6 | 30 | 751.65 | 1386 |

The relationship between the mean fracturing power and the total length of fractures is shown in Figure 15. The mean fracturing power has a good positive liner relationship with the fracture total length and the coefficient of determination is found to 0.9052. In most circumstances, especially in field, fractures cannot be observed and measured directly. And the fracture length is most important parameter to evaluate the hydraulic fracturing effect. Previous methods to the evaluate hydraulic fracturing are usually the drilling, micro-earthquake, and magnetotelluric method, these measurement methods sometimes cannot be used in field due to their high budget. As a result, estimating the fracture length is always a challenging work in field scale hydraulic fracturing. The fracture total length roughly positive increases with the increase of the mean fracturing power, hence we can use this relationship to roughly evaluate the fracture length in field with almost no cost. This linear relationship provides us with a new way to roughly predict fracture length.

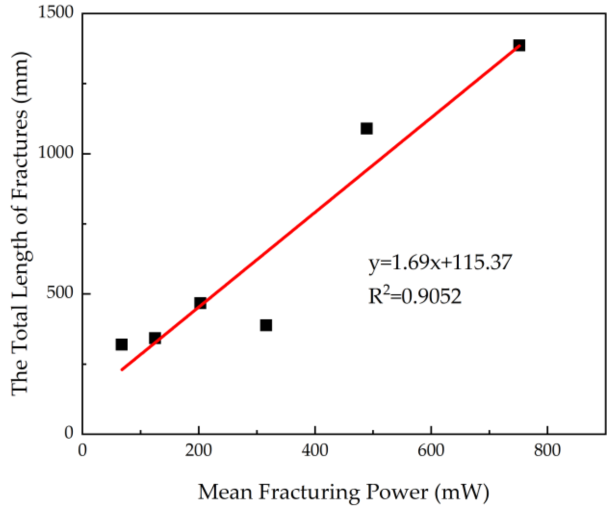


**Figure 15.** Influence of mean fracturing power on the fracture length.

*4.7. The Permeability of the Hydraulic Fracture*

Up until now, hydraulic fracturing is an imperative technique for economic exploitation of geothermal energy resources by enhancing deep buried rock permeability. Therefore, it is important to understand the permeability after hydraulic fracturing. Patel et al. [62] proposed a method to estimate fracture permeability using the injection pressure data. This method hypothesizes that due to the injected fracturing fluid flowing into induced fractures, a drop of the injection pressure happens just after the breakdown phenomenon. This hypothesizes is in accordance with our aforementioned pressure sharply decrease reason. Here, we used this method to analyze the fracture permeability of the rock samples after test.

Figure 8a–f show the pressure curves the six tests. In these curves, just after the breakdown pressure, a sharp decrease in injection pressure (pump pressure) is observed. The drop down of the pressure is caused by the injected fluid diffusion when water goes into the new created fracture volume. The diffusion source is the water outlet hole in the steel tube. After the sharp descend in the pressure curve, the injected fluid flows into the rock sample through induced fractures. Therefore the pressure will obey a one-dimensional diffusion equation:

$$\frac{\partial P}{\partial t} - D\frac{\partial^2 P}{\partial z^2} = 0, \tag{2}$$

The solution to Equation (2) could be given by Equation (3):

$$\triangle P(z,t) = P_0 erf\left(\frac{z}{\sqrt{4Dt}}\right), \tag{3}$$

where $t$ is the time after the breakdown, $D$ is the hydraulic diffusivity, $z$ is the length of the fracture, and $P_0$ is the breakdown pressure. Equation (3) can be used to modelling fit the experiment pressure curve, $P_0$, $z$, and $t$ are known and then the hydraulic diffusivity could be estimated. The induced fracture permeability could be estimated from Equation (3) through hydraulic diffusivity with the equation Shapiro et al. [63]:

$$D = \frac{NK}{\mu}, \tag{4}$$

where $\mu$ is the dynamic viscosity of the fluid, K is the permeability, and N is defined as:

$$N = \frac{MP_d}{H}, \tag{5}$$

where,

$$M = \frac{1}{\left(\frac{\phi}{K_f} + \frac{(\alpha-\phi)}{K_g}\right)}, \tag{6}$$

$$\alpha = 1 - \frac{K_d}{K_g}, \tag{7}$$

$$H = P_d + \alpha^2 M, \tag{8}$$

$$P_d = K_d + \frac{4}{3\mu_d}, \tag{9}$$

where $\mu_d$ is the shear modulus of the frame and $\phi$ is the porosity, $K_f$, $K_g$, and $K_d$ are the fluid bulk moduli, grain material, and dry frame, respectively.

Based on the Equations (2)–(9), the fracture permeability could be calculated by using hydraulic fracturing pressure curves of the six granite rock samples. The values of $K_f$, $K_g$, and $K_d$ are 2.18, 75, and 28.09 GPa, respectively. The $\mu_d$ and $\phi$ are 15.58 GPa and 0.0395 Pa·s, respectively, and the $\mu$ is 0.000,186,3 Pa·s.

The permeability was 0.92 1.21, 2.23, 3.32, 5.72, and 7.54 mD when injection flow rate was 5, 10, 15, 20, 25, and 30 mL/min, respectively. The value of estimated fracture permeability with injection flow rate is plotted in Figure 16. The fracture permeability shows a positively ascend trend with the injection flow rate increase. And it means that a higher injection flow rate will cause wider, lager fractures. All of the rock sample permeability after hydraulic fracturing is higher than the sample original permeability. As the original permeability is 0.34 mD, the permeability is obviously promoted. When the injection flow rate increases by 5 mL/min every time, compared with the original sample permeability, the permeability is increased 1.71, 2.55, 5.56, 8.78, 15.81, and 21.21 times, respectively. When the injection flow rate is 30 mL/min, the permeability is the highest. In field-scale operation, we usually trend to create more fractures and form higher permeability, a higher injection flow rate is better. At the same time, this also puts forward higher requirements for technology and equipment, it may require more cost and more advanced equipment, hence the maximum permeability as the primary consideration may not be economical nor reasonable. Therefore, in the hydraulic fracturing process, it is necessary to consider fracturing scheme carefully, the injection rate can not only form a good fracture network, obviously improve permeability, but also ensure a reasonable cost. For example, for the five fracturing injection rates selected in this experiment, the 25 mL/min can be considered as the best. Although 5, 10, 15, and 20 mL/min increased the permeability to a certain extent, but the magnitude of the permeability is not increased higher enough, a fracture network is not formed, the hydraulic fracturing effect is not obvious. Whereas the 30 mL/min has obtained the maximum permeability, compared with the permeability result of 25 mL/min, the permeability is increased 31.82%, this promotion is not obvious enough. Considering the cost of a field operation, this increase is unworthy, so the injection rate of 25 mL/min can be regarded as the best, of course, this conclusion is only the based on the experimental result. In field, more factors should be considered when selecting a reasonable injection flow rate.

Pate et al. [63] calculated hydraulic fracturing permeabilities, which are 2.28, 2.58, and 5.69 mD, when hydraulic diffusivities are 0.00086, 0.001075, and 0.00215, respectively. The estimated fracture permeabilities were compared with the fracture permeabilities measured by using AP608™ permeability test apparatus. Solberg et al. [19] analyzed the hydraulic fracturing in low permeability sandstone rocks with kinds of injection rates. The permeabilities of rock are measured and the change of permeability before and after the experiment is compared. Their research shows that hydraulic fracturing induced permanent structural changes in the rock and increased rock permeability. The permeabilities are 0.38, 5.99, 24.89, and 13.76 nm$^2$ correspond to the pump rates of 3.0, 15, 30, and 70 mm$^3$/s. The estimated permeabilities are in close agreement with the measured ones. Our experimental conclusions were consistent with the results of Solberg and Patel et al.

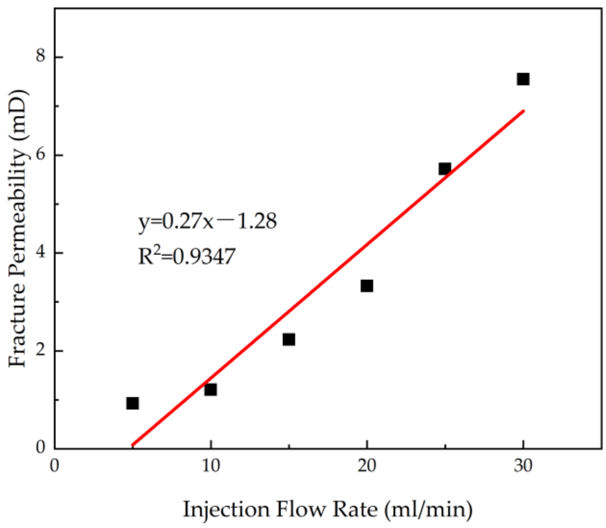


**Figure 16.** Influence of injection flow rate on the permeability

## 5. Application of the Methodology in Energy Mining

The rock reservoirs natural permeability is very low, and hence these reservoirs should be enhanced to stimulate efficient and economic mining. Hydraulic fracturing, as a promising method to improving in situ permeability, fluid flow, and extraction efficiency, provides a sustained injection and circulation technology for prospects of commercial extracting petroleum and geothermal heat from deep buried reservoir. The core technology of hydraulic fracturing is choosing a reasonable injection flow rate and pressure to enhance permeability and create new fractures. Our research results show that a high injection rate trend to cause a relatively complex induced fracture network. At the same time, high injection rates also correspond to high breakdown pressures, high initiation pressures, long propagation times, and low revised post-fracturing pressures, the initiation pressures could be used to estimate failure stresses, the propagation times are related to the induced earthquakes, the post-fracturing pressures influences the heat extraction efficiency. Therefore, we cannot only consider breakdown pressure when designing fracturing scheme, whereas should consider the influence of different parameters on the fracturing results, induced earthquakes and heat extraction efficiency in situ when choosing injection flow rates.

Because of the limitation of experiment conditions, our experimental study contains some shortcomings: for instance, as just mentioned, even if we know the injection flow rate is not the higher the better, we do not know how to choose an injection flow rate and how much permeability is optimal. This work needs further research.

## 6. Conclusions

In this paper, we use true-triaxial hydraulic fracturing laboratory testing with large-size granite samples to investigate hydraulic fracturing characteristics by varying the injection flow rate. According to the cut granite samples and the pressure data, we analyzed the fracture initiation pressure, propagation time, post-fracturing pressure, breakdown pressure, fracture geometry, and length. The fracture permeability was calculated at last. The conclusions obtained are list below:

(1) A particular pressure–time curve could be divided into four main phases: initial pressure development stage, wellbore pressurization stage, fracturing phase, and post-failure stage. The pressurization rate curve could help to distinguish the four phases. Four parameters of the fracture initiation pressure, propagation time, post-fracturing pressure, and breakdown pressure could be obtained from the pressure–time curves. The injection flow rates significantly influenced these four parameters during hydraulic fracturing. The initiation pressures and breakdown

pressures have approximately linear positive relations to injection flow rates. The post-fracturing pressure and propagation time had approximately linear negative relations to injection flow rates.

(2) When the injection flow rate is low, fracture propagation direction is along the PFD under the control of triaxial stresses. With the increase of injection flow rate, the fracture initiation is like a kind of "exploded" phenomenon, the energy and pressure are released rapidly, and the fracture propagation direction sometimes is not along the PFD near the wellbore zone because of the complex stress state. When the fracture propagates away from the stress complex zone, its direction is influenced by triaxial stresses (crustal stress in field) again and will gradually turn to PFD as the fracture grows.

(3) The total length of the fractures increases with the increase of injection flow rate, and when the injection flow rate is low, mainly shear fractures are induced, and the hydraulic fracturing may not cause a fracture network. As the injection flow rate increases, when the tension fractures dominate fracturing patterns, the hydraulic fracturing tends to form a complex fracture network. The width of the fracture also increases with the increase of injection flow rate, a wider fracture system will result in lesser frictional resistance for fluid flowing and a higher permeability.

(4) A parameter of Mean Fracturing Power is proposed to estimate the fracture total length. This parameter represents the power injected into rock for fracture propagation. The fracture total length almost linearly increases with the increase of Mean Fracturing Power and this linear relationship provided us with a way to roughly predict fracture length.

(5) The fracture permeability of rock samples after hydraulic fracturing shows a linear ascending trend with the increase of the injection flow rates.

In the future work of this study, we will numerically simulate the hydraulic induced fracture propagation by the discrete element method, especially analyzing the influence of injection flow rate on the fracture patterns. Then, we will compare the numerical results with the experimental results, and try to find a numerical model which could be used in field-scale operation. In addition, we will try to find out which injection flow rate and permeability is optimal for field-scale hydraulic fracturing. The connection of existing natural fractures is also part of our future study.

**Author Contributions:** Y.C. and Y.Z. conceived and designed the experiments; Y.C. performed the experiments and wrote the paper. All authors have read and agreed to the published version of the manuscript.

**Funding:** This research was funded by the National Key Research and Development Program of China, Topic 3 (NO.2018YFB1501803), the National Natural Science Foundation of China (No.41772238).

**Conflicts of Interest:** The authors declare no conflict of interest.

## References

1. Chong, Z.H.; Yao, Q.L.; Li, X.H. Experimental Investigation of Fracture Propagation Behavior Induced by Hydraulic Fracturing in Anisotropic Shale Cores. *Energies* **2019**, *12*, 976. [CrossRef]
2. Jing, F.; Sheng, Q.; Luo, C.W.; Zeng, J. The application of hydraulic fracturing in storage projects of liquefied petroleum gas. *Key Eng. Mat.* **2006**, *306–308*, 1509–1514. [CrossRef]
3. Zhao, X.; He, E.J.; Guo, J.C.; Zhu, H.Y.; Wang, H.H.; He, W. The study of fracture propagation in pre-acidized shale reservoir during the hydraulic fracturing. *J. Petrol. Sci. Eng.* **2020**, *184*, 106488. [CrossRef]
4. Tan, P.; Pang, H.W.; Zhang, R.X.; Jin, Y.; Zhou, Y.C.; Kao, J.W.; Fan, M. Experimental investigation into hydraulic fracture geometry and proppant migration characteristics for southeastern Sichuan deep shale reservoirs. *J. Petrol. Sci. Eng.* **2020**, *184*, 106517. [CrossRef]
5. Osborn, S.G.; Vengosh, A.; Warner, N.R.; Jackson, R.B. Methane contamination of drinking water accompanying gas-well drilling and hydraulic fracturing. *Proc. Natl. Acad. Sci. USA* **2011**, *108*, 8172–8176. [CrossRef]
6. Cahill, A.G.; Steelman, C.M.; Forde, O.; Kuloyo, O.; Ruff, S.E.; Mayer, B.; Mayer, K.U.; Strous, M.; Ryan, M.C.; Cherry, J.A. Mobility and persistence of methane in groundwater in a controlled-release field experiment. *Nat. Geosci.* **2017**, *10*, 289–294. [CrossRef]

7. Taherdangkoo, R.; Tatomir, A.; Taylor, R.; Sauter, M. Numerical investigations of upward migration of fracking fluid along a fault zone during and after stimulation. *Energy Procedia* **2017**, *125*, 126–135. [CrossRef]
8. Taherdangkoo, R.; Tatomir, A.; Anighoro, T.; Sauter, M. Modeling fate and transport of hydraulic fracturing fluid in the presence of abandoned wells. *J. Contam. Hydrol.* **2019**, *221*, 58–68. [CrossRef]
9. Giardini, D. Geothermal quake risks must be faced. *Nature* **2009**, *462*, 848–849. [CrossRef]
10. Trifu, C.I. Special issue: The mechanism of induced seismicity - Introduction. *Pure Appl. Geophys.* **2002**, *159*, 1–5.
11. Guo, F.; Morgenstern, N.; Scott, J. Interpretation of hydraulic fracturing breakdown pressure. *Int. J. Rock Mech. Min. Sci.* **1993**, *30*, 617–626. [CrossRef]
12. Santillán, D.; Juanes, R.; Cueto-Felgueroso, L. Phase field model of hydraulic fracturing in poroelastic media: Fracture propagation, arrest, and branching under fluid injection and extraction. *J. Geophys. Res. Solid Earth* **2018**, *123*, 2127–2155. [CrossRef]
13. Rothert, E.; Shapiro, S.A. Statistics of fracture strength and fluid-induced microseismicity. *J. Geophys. Res. Solid Earth* **2007**, *112*. [CrossRef]
14. Zoback, M.D.; Harjes, H.-P. Injection-induced earthquakes and crustal stress at 9 km depth at the KTB deep drilling site, Germany. *J. Geophys. Res. Solid Earth* **1997**, *102*, 18477–18491. [CrossRef]
15. Zoback, M.; Rummel, F.; Jung, R.; Raleigh, C. Laboratory hydraulic fracturing experiments in intact and pre-fractured rock. *Int. J. Rock Mech. Min. Sci. Geomech.* **1977**, *14*, 49–58. [CrossRef]
16. Hubbert, M.K.; Willis, D.G. Mechanics of hydraulic fracturing. In *Underground Waste Management and Environmental Implications*; Society of Petroleum Engineers: Richardson, TX, USA, 1972.
17. Haimson, B.; Fairhurst, C. Initiation and extension of hydraulic fractures in rocks. *Soc. Pet. Eng. J.* **1967**, *7*, 310–318. [CrossRef]
18. Haimson, B.; Fairhurst, C. Hydraulic fracturing in porous-permeable materials. *J. Pet. Technol.* **1969**, *21*, 811–817. [CrossRef]
19. Solberg, P.; Lockner, D.; Byerlee, J. Hydraulic fracturing in granite under geothermal conditions. *Int. J. Rock Mech. Min.* **1980**, *17*, 25–33. [CrossRef]
20. Solberg, P.; Lockner, D.; Byerlee, J. Shear and tension hydraulic fractures in low permeability rocks. *Pure Appl. Geophys.* **1977**, *115*, 191–198. [CrossRef]
21. Frash, L.P.; Gutierrez, M.; Hampton, J. True-triaxial apparatus for simulation of hydraulically fractured multi-borehole hot dry rock reservoirs. *Int. J. Rock Mech. Min. Sci.* **2014**, *70*, 496–506. [CrossRef]
22. Lockner, D.; Byerlee, J. Hydrofracture in Weber sandstone at high confining pressure and differential stress. *J. Geophys. Res.* **1977**, *82*, 2018–2026. [CrossRef]
23. Song, I.; Suh, M.; Won, K.S.; Haimson, B. A laboratory study of hydraulic fracturing breakdown pressure in tablerock sandstone. *Geosci. J.* **2001**, *5*, 263–271. [CrossRef]
24. Patel, S.; Sondergeld, C.; Rai, C. Laboratory studies of hydraulic fracturing by cyclic injection. *Int. J. Rock Mech. Min. Sci.* **2017**, *95*, 8–15. [CrossRef]
25. Fallahzadeh, S.; Hossain, M.; James Cornwell, A.; Rasouli, V. Near Wellbore Hydraulic Fracture Propagation from Perforations in Tight Rocks: The Roles of Fracturing Fluid Viscosity and Injection Rate. *Energies* **2017**, *10*. [CrossRef]
26. Nagel, N.B.; Gil, I.; Sanchez-Nagel, M.; Damjanac, B. Simulating hydraulic fracturing in real fractured rocks-overcjavascript: Itermoming the limits of pseudo3D models. In Proceedings of the SPE Hydraulic Fracturing Technology Conference, Society of Petroleum Engineers, The Woodlands, TX, USA, 24–26 January 2011.
27. Zhang, X.; Jeffrey, R. Development of fracture networks through hydraulic fracture growth in naturally fractured reservoirs. In Proceedings of the ISRM International Conference for Effective and Sustainable Hydraulic Fracturing, Brisbane, Australia, 20–22 May 2013.
28. Al-Busaidi, A.; Hazzard, J.F.; Young, R.P. Distinct element modeling of hydraulically fractured Lac du Bonnet granite. *J. Geophys Res. Solid Earth* **2005**, *110*, B06302. [CrossRef]
29. Weng, X.; Kresse, O.; Cohen, C.; Wu, R.; Gu, H. Modeling of Hydraulic-Fracture-Network Propagation in a Naturally Fractured Formation. *SPE Prod. Oper.* **2011**, *26*, 368–380. [CrossRef]
30. Rothert, E.; Shapiro, S.A. Microseismic monitoring of borehole fluid injections: Data modeling and inversion for hydraulic properties of rocks. *Geophysics* **2003**, *68*, 685–689. [CrossRef]

31. Rahman, M.M.; Rahman, S.S. Studies of Hydraulic Fracture-Propagation Behavior in Presence of Natural Fractures: Fully Coupled Fractured-Reservoir Modeling in Poroelastic Environments. *Int. J. Geomech.* **2013**, *13*, 809–826. [CrossRef]
32. Guo, T.K.; Qu, Z.Q.; Gong, D.Q.; Lei, X.; Liu, M. Numerical simulation of directional propagation of hydraulic fracture guided by vertical multi-radial boreholes. *J. Nat. Gas Sci. Eng.* **2016**, *35*, 175–188. [CrossRef]
33. Pakzad, R.; Wang, S.Y.; Sloan, S.W. Numerical Simulation of Hydraulic Fracturing in Low-/High-Permeability, Quasi-Brittle and Heterogeneous Rocks. *Rock Mech. Rock Eng.* **2018**, *51*, 1153–1171. [CrossRef]
34. Deng, J.Q.; Lin, C.; Yang, Q.; Liu, Y.R.; Tao, Z.F.; Duan, H.F. Investigation of directional hydraulic fracturing based on true tri-axial experiment and finite element modeling. *Comput. Geotech.* **2016**, *75*, 28–47. [CrossRef]
35. Fan, T.-G.; Zhang, G.-Q. Laboratory investigation of hydraulic fracture networks in formations with continuous orthogonal fractures. *Energy* **2014**, *74*, 164–173. [CrossRef]
36. Kumari, W.G.P.; Ranjith, P.G.; Perera, M.S.A.; Li, X.; Li, L.H.; Chen, B.K.; Isaka, B.L.A.; De Silva, V.R.S. Hydraulic fracturing under high temperature and pressure conditions with micro CT applications: Geothermal energy from hot dry rocks. *Fuel* **2018**, *230*, 138–154. [CrossRef]
37. Ma, X.; Zoback, M.D. Laboratory experiments simulating poroelastic stress changes associated with depletion and injection in low-porosity sedimentary rocks. *J. Geophys. Res. Solid Earth* **2017**, *122*, 2478–2503. [CrossRef]
38. Zhuang, L.; Kim, K.Y.; Jung, S.G.; Diaz, M.; Min, K.B. Effect of Water Infiltration, Injection Rate and Anisotropy on Hydraulic Fracturing Behavior of Granite. *Rock Mech. Rock Eng.* **2019**, *52*, 575–589. [CrossRef]
39. Liu, H.; Chi, X.Y.; Li, W. Tectono-paleogeographic study of the early cretaceous in the Songliao Basin. *Min. Sci. Technol. (China)* **2011**, *21*, 93–98.
40. Mao, R.B.; Feng, Z.J.; Liu, Z.H.; Zhao, Y.S. Laboratory hydraulic fracturing test on large-scale pre-cracked granite specimens. *J. Nat. Gas Sci. Eng.* **2017**, *44*, 278–286. [CrossRef]
41. Huang, J.S.; Griffiths, D.V.; Wong, S.W. Initiation pressure, location and orientation of hydraulic fracture. *Int. J. Rock Mech. Min. Sci.* **2012**, *49*, 59–67. [CrossRef]
42. Xie, L.M.; Min, K.B. Hydraulic fracturing initiation and propagation in deep inclined open hole for Enhanced Geothermal System. *Geothermics* **2017**, *70*, 351–366. [CrossRef]
43. Baumgärtner, J.; Zoback, M.D. Interpretation of hydraulic fracturing pressure-time records using interactive analysis methods. *Int. J. Rock Mech. Min.* **1989**, *26*, 461–469. [CrossRef]
44. Fallahzadeh, S.H.; Rasouli, V.; Sarmadivaleh, M. An Investigation of Hydraulic Fracturing Initiation and Near-Wellbore Propagation from Perforated Boreholes in Tight Formations. *Rock Mech. Rock Eng.* **2015**, *48*, 573–584. [CrossRef]
45. Cornet, F.H. Earthquakes induced by fluid injections. *Science* **2015**, *348*, 1204–1205. [CrossRef] [PubMed]
46. McGarr, A. Maximum magnitude earthquakes induced by fluid injection. *J. Geophys. Res. Solid Earth* **2014**, *119*, 1008–1019. [CrossRef]
47. Lu, S.M. A global review of enhanced geothermal system (EGS). *Renew. Sustain. Energy Rev.* **2018**, *81*, 2902–2921. [CrossRef]
48. Zhuang, L.; Kim, K.Y.; Jung, S.G.; Diaz, M.; Min, K.B.; Zang, A.; Stephansson, O.; Zimmerman, G.; Yoon, J.S.; Hofmann, H. Cyclic hydraulic fracturing of pocheon granite cores and its impact on breakdown pressure, acoustic emission amplitudes and injectivity. *Int. J. Rock Mech. Min. Sci.* **2019**, *122*, 104065. [CrossRef]
49. Grigoli, F.; Cesca, S.; Rinaldi, A.P.; Manconi, A.; Lopez-Comino, J.A.; Clinton, J.F.; Westaway, R.; Cauzzi, C.; Dahm, T.; Wiemer, S. The November 2017 M-w 5.5 Pohang earthquake: A possible case of induced seismicity in South Korea. *Science* **2018**, *360*, 1003–1006. [CrossRef]
50. Kim, K.H.; Ree, J.H.; Kim, Y.; Kim, S.; Kang, S.Y.; Seo, W. Assessing whether the 2017 M-w 5.4 Pohang earthquake in South Korea was an induced event. *Science* **2018**, *360*, 1007–1009. [CrossRef]
51. Jeffrey, R.G.; Chen, Z.R.; Zhang, X.; Bunger, A.P.; Mills, K.W. Measurement and Analysis of Full-Scale Hydraulic Fracture Initiation and Reorientation. *Rock Mech. Rock Eng.* **2015**, *48*, 2497–2512. [CrossRef]
52. Legarth, B.; Huenges, E.; Zimmermann, G. Hydraulic fracturing in a sedimentary geothermal reservoir: Results and implications. *Int. J. Rock Mech. Min. Sci.* **2005**, *42*, 1028–1041. [CrossRef]
53. Hou, P.; Gao, F.; Ju, Y.; Yang, Y.G.; Gao, Y.N.; Liu, J. Effect of water and nitrogen fracturing fluids on initiation and extension of fracture in hydraulic fracturing of porous rock. *J. Nat. Gas Sci. Eng.* **2017**, *45*, 38–52. [CrossRef]
54. Hossain, M.M.; Rahman, M.K.; Rahman, S.S. Hydraulic fracture initiation and propagation: Roles of wellbore trajectory, perforation and stress regimes. *J. Petrol. Sci. Eng.* **2000**, *27*, 129–149. [CrossRef]

55. Tan, P.; Jin, Y.; Han, K.; Hou, B.; Chen, M.; Guo, X.F.; Gao, J. Analysis of hydraulic fracture initiation and vertical propagation behavior in laminated shale formation. *Fuel* **2017**, *206*, 482–493. [CrossRef]
56. Fatahi, H.; Hossain, M.M.; Fallahzadeh, S.H.; Mostofi, M. Numerical simulation for the determination of hydraulic fracture initiation and breakdown pressure using distinct element method. *J. Nat. Gas Sci Eng.* **2016**, *33*, 1219–1232. [CrossRef]
57. Zhang, Y.S.; Zhang, J.C.; Yuan, B.; Yin, S.X. In-situ stresses controlling hydraulic fracture propagation and fracture breakdown pressure. *J. Petrol. Sci. Eng.* **2018**, *164*, 164–173. [CrossRef]
58. Chen, M.; Jiang, H.; Zhang, G.Q.; Jin, Y. The Experimental Investigation of Fracture Propagation Behavior and Fracture Geometry in Hydraulic Fracturing through Oriented Perforations. *Petrol. Sci. Technol.* **2010**, *28*, 1297–1306. [CrossRef]
59. Jin, X.; Shah, S.N.; Roegiers, J.-C.; Hou, B. Breakdown Pressure Determination-a Fracture Mechanics Approach. In Proceedings of the SPE Annual Technical Conference and Exhibition, New Orleans, LA, USA, 30 October 2013.
60. Haimson, B.; Huang, X. Hydraulic Fracturing Breakdown Pressure and In Situ Stress at Great Depth. In Proceedings of the ISRM International Symposium, Pau, France, 30 September 1989.
61. Hofmann, H.; Babadagli, T.; Zimmermann, G. Numerical Simulation of Complex Fracture Network Development by Hydraulic Fracturing in Naturally Fractured Ultratight Formations. *J. Energ. Resour.-Asme* **2014**, *136*, 042905. [CrossRef]
62. Patel, S.M.; Sondergeld, C.H.; Rai, C.S. Hydraulic fracture permeability estimation using stimulation pressure data. *Int. J. Rock Mech. Min. Sci.* **2018**, *101*, 50–53. [CrossRef]
63. Shapiro, S.A.; Patzig, R.; Rothert, E.; Rindschwentner, J. Triggering of seismicity by pore-pressure perturbations: Permeability-related signatures of the phenomenon. *Pure Appl. Geophys.* **2003**, *160*, 1051–1066. [CrossRef]